

FPGA-Based Neural Network Accelerators for Space Applications: A Survey

Pedro Antunes¹ and Artur Podobas²

¹pedroa@kth.se

²podobas@kth.se

ABSTRACT

Space missions are becoming increasingly ambitious, necessitating high-performance onboard spacecraft computing systems. In response, field-programmable gate arrays (FPGAs) have garnered significant interest due to their flexibility, cost-effectiveness, and radiation tolerance potential. Concurrently, neural networks (NNs) are being recognized for their capability to execute space mission tasks such as autonomous operations, sensor data analysis, and data compression. This survey serves as a valuable resource for researchers aiming to implement FPGA-based NN accelerators in space applications. By analyzing existing literature, identifying trends and gaps, and proposing future research directions, this work highlights the potential of these accelerators to enhance onboard computing systems.

Keywords: Artificial Intelligence (AI), Neural Networks (NN), Neuromorphic Computing, Field Programmable Gate Arrays (FPGAs), Hardware Accelerators, Space Missions

1 INTRODUCTION

Space, the final frontier, has captivated human curiosity since ancient times. The advent of the space race marked a significant milestone, leading to the deployment of spacecraft across nearly every celestial body within our solar system, including Mars (Viking 1/2), Venus (Venera 7), Mercury (Mariner 10), Jupiter (Galileo), Saturn (Cassini), and various moons (e.g., Apollo 11, Phobos 2). This exploration continues to expand with numerous ongoing and upcoming missions¹. Concurrently, the decreasing cost of space launches [78] has resulted in an exponential increase in the deployment of small satellites, such as Nanosatellites or Cubesatellites, into Earth's orbit [88] – a trend showing no signs of abatement.

Central to every spacecraft, from nanosatellites to deep-space rockets, is some form of electrical component responsible for computation. These computations range from systems that manage spacecraft steering and navigation (e.g., the Apollo Guidance Computer [131]) to those analyzing vast data streams generated by advanced sensors. As missions become more ambitious and data volumes grow, the demand for high-performance onboard computing becomes increasingly critical.

Currently, a significant portion of onboard computing is facilitated through field-programmable gate arrays (FPGAs) [89]. These reconfigurable electrical components can be programmed with various types of computing elements, from small digital signal processing (DSP) blocks to large central processing units (CPUs). FPGAs offer several advantages over commercial off-the-shelf components (COTS), such as CPUs or graphical processing units (GPUs): they are cost-effective for low-volume production, consume less energy and power, exhibit radiation tolerance/hardening, and provide numerous options for fault-tolerant designs. These attributes – particularly their energy efficiency and resilience – are crucial in the harsh, radiation-intensive space environment with limited thermal dissipation capabilities. Traditionally used to run imperative applications, FPGAs are increasingly employed within a different computational paradigm: Neural Networks (NNs) [91].

The application of NNs in spacecraft has been contemplated since Deep-Space 1 [63], where it was considered among thirteen emerging technologies for autonomous operation and navigation. With the advancement and refinement of deep learning techniques, NNs have garnered renewed interest for space system applications. These networks can potentially enhance various domains such as autonomous operation and navigation, sensor analysis [142], data compression [54], and selective downlinking [184],

¹<https://www.astronomy.com/space-exploration/space-missions-a-list-of-current-and-upcoming-voyages/>

addressing the challenge of slow data transmission from spacecraft.

This systematic survey synthesizes existing literature on FPGA-based NN accelerators in space, identifying trends, gaps, and future directions within this burgeoning field. Although numerous excellent surveys exist concerning NNs [168], sensors [68], FPGAs (specifically for CNNs) [122], and space applications [98, 26], to our knowledge, this is the first comprehensive and systematic study focusing specifically on FPGA-based NN accelerators for space.

The remainder of this paper is structured as follows: Section 2 provides essential background information to contextualize the literature; Section 3 outlines the survey methodology and summarizes the reviewed literature; Section 4 discusses key findings and insights derived from the literature review; Section 5 presents unexplored or underexplored research areas identified in the literature; and Section 6 concludes this work.

2 BACKGROUND

Space missions are inherently complex and require efficient and reliable computing systems. They can be broadly categorized into near-Earth orbit or deep space missions [12]. Near-Earth orbits include Low Earth Orbit (LEO), Medium Earth Orbit (MEO), and Geostationary Earth Orbit (GEO). LEO is between 160 km to 1000 km above the Earth's surface. The Starlink system is an example of a LEO constellation [120]. MEO is between 1,000 km and 35,786 km above the Earth's surface. The European Galileo system is an example of an MEO mission ². GEO is approximately 35,786 km above the Earth's surface. The ESA's European Data Relay System (EDRS) is an example of a GEO mission ³. Deep space missions extend beyond these orbits, with the Moon often considered the lower boundary for deep space.

The environments within these orbital categories differ significantly, affecting spacecraft in various ways [72]. One key difference is radiation levels, which pose risks to hardware components and can degrade overall system performance [39]. As a result, hardware must be designed with fault tolerance to mitigate these effects and ensure reliable functionality. Additional factors, such as energy sources, temperature fluctuations, and vibrations during the mission [169], also play a role in spacecraft design. However, this paper will focus on a hardware logic perspective, and further discussion of these additional concerns lies beyond its scope.

2.1 Hardware Systems for Space Missions

Satellite hardware systems integrate flexible and high-performance components such as Central Processing Units (CPUs), Graphics Processing Units (GPUs), FPGAs, and Neuromorphic Processing Units (NPU) (Figure 1). While commercial off-the-shelf (COTS) versions of these components may be utilized for short-lived space missions, they are typically inadequate for harsh radiation environments. These environments expose hardware to radiation from galactic cosmic rays (GCRs) and solar-weather events such as solar winds, flares, and coronal mass ejections (CMEs). Such radiation can induce short-term effects, known as Single Event Effects (SEEs), and long-term effects, compromising mission success. To mitigate these radiation-induced effects, manufacturers provide fault-tolerant devices. Although these devices are more costly and have reduced performance compared to COTS components, they enhance reliability in space applications [129].

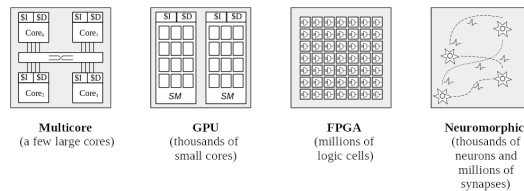


Figure 1. Abstract comparison of CPU, GPU, FPGA, and NPU.

Fault-tolerance strategies in computer science are categorized into three primary methods (Figure 2): (i) fault mitigation, (ii) fault detection, and (iii) fault repair [178]. **Fault mitigation** techniques aim to

²<https://www.euspa.europa.eu/eu-space-programme/galileo>

³<https://connectivity.esa.int/european-data-relay-satellite-system-edrs-overview>

prevent the propagation of radiation effects. Examples include employing radiation-hardened or radiation-tolerant devices with microelectronic materials treated to withstand specific total ionizing dose (TID) levels [11, 80]. Another prevalent technique is FPGA scrubbing, which limits the impact of SEEs through methods such as blind, read-back, and hybrid scrubbing. Blind scrubbing involves periodic error-free scrubbing of the FPGA, while read-back scrubbing occurs upon detecting an SEE. Hybrid scrubbing combines both approaches. These methods can be applied to the full configuration memory or only partially in the affected area [64].

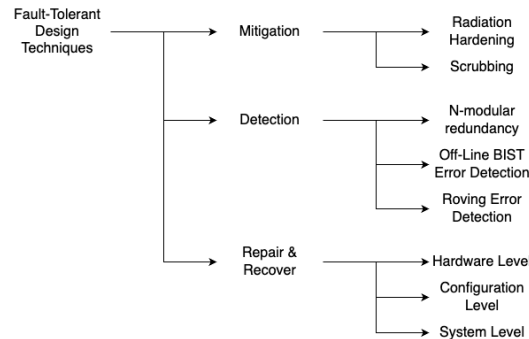


Figure 2. Tree representation of the different fault tolerance design techniques.

Fault detection techniques identify the occurrence of SEEs. One such method is N-modular redundancy (NMR), commonly implemented as double or triple-modular redundancy (DMR and TMR, respectively) [87]. DMR duplicates a circuit and compares its output, triggering an error if discrepancies arise. TMR involves triplication with a voting procedure that allows operations using the majority value while flagging errors. Another fault detection method is built-in self-test (BIST) error detection [3], which verifies system outputs against known values for specific inputs. This method temporarily halts full system operation during testing. Roving error detection [2] overcomes this limitation by executing BIST on individual circuit segments, allowing normal operation elsewhere and providing precise fault localization.

Fault repair techniques address hardware issues caused by SEEs through various approaches. At the hardware level, faulty components are replaced with pre-designed spare parts within the architecture, constrained by design component limits. For FPGAs and reconfigurable systems, configuration-level techniques allow the reconfiguration of affected components to alternative designs upon fault detection. System-level redundancy involves either performance reduction using alternate components or system duplication on spacecraft.

The selection of hardware components depends on mission-specific requirements. CPUs are favored for their flexibility, while GPUs are preferred for highly parallelizable tasks requiring high performance, such as image processing. FPGAs balance customization and cost-effectiveness, making them attractive for many space missions. NPU are relatively new and can potentially revolutionize AI applications in space missions due to their power efficiency.

2.2 Reconfigurable Hardware Systems

Reconfigurable architectures represent systems that preserve some degree of silicon flexibility typically forfeited by application-specific integrated circuits (ASICs). Their reconfigurability can manifest at different levels of granularity [139], with field-programmable gate arrays (FPGAs) providing the most prevalent and fine-grained option.

FPGAs feature thousands or millions of look-up tables (LUTs), programmable interconnects, and Input/Output (I/O) pads (Figure 3). By programming these LUTs with specific Boolean functions and the interconnects, digital designs such as central processing units (CPUs), digital signal processors (DSPs), and custom accelerators can be realized. While early iterations of FPGAs solely contained LUTs, modern models also integrate hardened DSP blocks that enhance computational capabilities and incorporate on-chip static random access memory (SRAM). These versatile devices are employed across diverse computing domains, including ASIC prototyping, telecommunications, low-volume consumer electronics, high-performance computing, and notably, space applications. Some systems combine FPGAs with hard

processor cores, resulting in System-on-Chip configurations encompassing programmable logic (PL) and a processing system (PS).

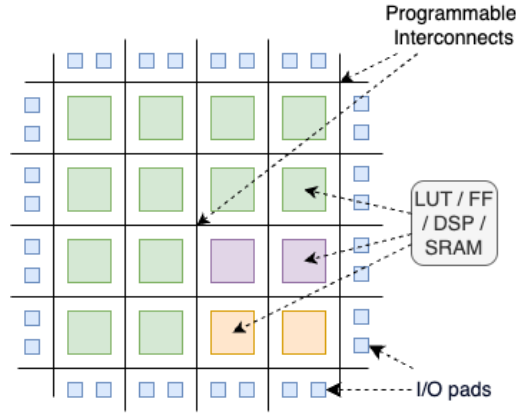


Figure 3. Abstract representation of the structure of an FPGA, showing logic blocks, programmable interconnect, and IO pad.

FPGAs offer several advantages for space applications compared to other hardware solutions such as CPUs or ASICs: (i) they are significantly more economical, being orders of magnitude cheaper than manufacturing ASICs; (ii) they can be designed with radiation tolerance or hardening, enhancing resilience against errors relative to alternative hardware options; (iii) their reconfigurability permits the remote deployment of patches or firmware updates and facilitates bug remediation; (iv) they provide a reduced time-to-market compared to ASICs [15].

Two primary methodologies exist for designing systems on FPGAs. The first involves using hardware description languages (HDLs), such as VHDL, Verilog, or Chisel, to manually detail designs at the Register Transfer Level (RTL). This approach offers precise control over design descriptions but is accompanied by a steep learning curve. Alternatively, logic can be described using abstract programming languages like C/C++ to define functionality. This method employs High-Level Synthesis (HLS) tools, such as Vitis HLS⁴ or Intel OpenCL [33], which transform abstract C code into RTL. Although HLS tools present a less daunting learning curve, they provide reduced control over the generated hardware due to many decisions being delegated to the HLS compiler. Recently, HLS tools targeting NNs have emerged, enabling NN descriptions in frameworks such as PyTorch or ONNX and their subsequent synthesis into hardware. An example of this type of tool is FINN [163].

2.3 Neural Networks

Traditional artificial neural networks/deep neural networks (ANNs/DNNs) [92] are grounded in the concept of a perceptron [118], an abstract model of a real neuron. This foundational concept paved the way for multi-layer perceptron (MLP) [140] networks. Subsequently, Convolutional Neural Networks (CNNs) emerged [46], incorporating convolutional, pooling, fully-connected, and activation layers. Each connection between neurons is associated with a weight in these networks, and each neuron may have an associated bias. These weights and biases constitute the parameters of a NN, typically represented using floating-point arithmetic. Given that a NN can encompass billions of parameters, with each floating-point number occupying 4 Bytes in memory, efforts to reduce their memory footprint through quantization have been pursued [52]. Quantization allows for parameter width reduction down to 1-bit, leading to the development of binarized neural networks (BNNs) [30]. Each layer within these networks entails a specific set of operations; for instance, a convolutional layer involves multiplications and accumulations. The number of operations in such a layer is calculated as described in Equation 1:

$$\text{Operations} = 2 \times (\text{Kernel Width} \times \text{Kernel Height} \times \text{Input Channels}) \times \text{Output Channels} \times \text{Output Width} \times \text{Output Height} \quad (1)$$

⁴<https://www.amd.com/en/products/software/adaptive-socs-and-fpgas/vitis/vitis-hls.html>

where the kernel width and height refer to the dimensions of the convolutional kernel, input channels represent the number of channels in the input feature map, output channels denote the number of filters in the convolutional layer, and output width and height correspond to the dimensions of the output feature map. The factor of 2 accounts for both multiplication and accumulation operations. For a fully connected (FC) layer, the number of operations is given by Equation 2:

$$\text{Operations} = 2 \times (\text{Input Size}) \times (\text{Output Size}) \quad (2)$$

The input size refers to the number of neurons in the previous layer, and the output size corresponds to the number of neurons in the current layer. An NN's total number of operations is the aggregate of operations across all layers.

More recently, spiking neural networks (SNNs) [113] have been introduced as the third-generation ANNs, drawing greater inspiration from biological neurons in human or animal brains. In SNNs, neurons often function as leaky integrators and communicate primarily through events known as spikes.

Various NN types are constructed by connecting neurons and layers in diverse configurations. This survey highlights some key types of NNs: classification (yielding a single class label or a probability distribution over multiple classes), segmentation (producing pixel-wise class labels for segmented images), object detection (outputting bounding boxes with class labels and confidence scores), generative networks (generating new images, text, or other content), keypoint detection (identifying specific coordinate points in an image), depth estimation (creating a depth map with continuous values per pixel), and Q-learning (outputting Q-values for all possible actions).

This survey categorizes training as either online or offline and supervised or unsupervised. Online training involves updating the NN's weights on the same device performing inference. In contrast, offline training occurs when the NN is trained on a separate device before being deployed solely for inference. Supervised learning entails providing expected outputs/labels during training, while unsupervised learning involves training with unlabeled data. Traditional perceptron-based systems are predominantly trained offline at data centers in a supervised manner—an expensive operation impractical for deep space missions. Conversely, SNNs often undergo unsupervised training, enabling space missions to potentially adapt their classification algorithms to novel circumstances when sensors detect previously unclassified phenomena.

2.4 FPGA-based Neural Network Accelerators

In this survey, we categorize FPGA-based NN accelerators into two primary architectural paradigms: dataflow architecture and time-multiplexed architecture. The former maps all NN layers onto the FPGA fabric, as illustrated in Figure 4. Conversely, the latter defines multiple processing elements (PEs), which are reused to compute different layers within the NN, depicted in Figure 5.

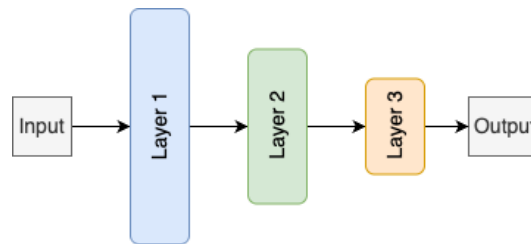


Figure 4. Dataflow architecture of an FPGA-based NN accelerator.

The inference latency of these accelerators is defined as the time required for an NN input to propagate through to its output. In scenarios where only a single input is processed at any given moment, the throughput, typically expressed in frames per second (FPS), is inversely proportional to this inference time. Additionally, accelerator performance can be quantified by the number of operations executed per second (OP/s), which is derived from multiplying the throughput by the total operations performed by the NN model during inference.

Power consumption measurements are crucial and should be conducted while the accelerator performs inference tasks. Generally, power consumption is predominantly influenced by the number of bit flips occurring during design execution. Lower frequency operation or reduced resource utilization can lead to

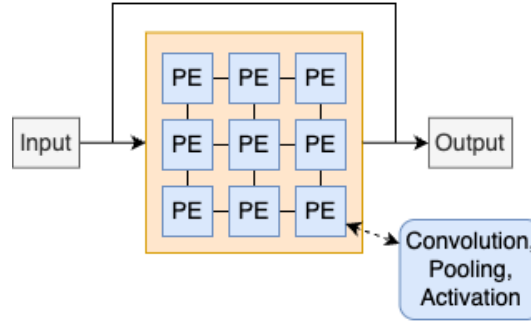


Figure 5. Time-multiplexed architecture of an FPGA-based NN accelerator.

decreased power consumption. Energy consumption, on the other hand, is calculated by multiplying the power consumption by the inference time.

Furthermore, when considering applications within space environments, an essential performance metric is the number of operations executed per second per watt (OP/s/W). This metric provides a comprehensive understanding of the efficiency and suitability of FPGA-based NN accelerators in resource-constrained settings.

3 LITERATURE REVIEW

This section examines various papers, providing a chronological summary based on publication date. These papers were identified using a carefully crafted search string 1 across the Web of Science, Scopus, IEEE Digital Library, and ACM Digital Library and filtered to align with this survey's objectives. Additionally, references from reviewed papers and Google Scholar searches supplemented these results.

The analysis focused on several key aspects within the relevant literature. Initially, we examined each paper's introduction to understand how authors contextualized their work within the field, identified the problem addressed, and presented solutions or extended existing research. Subsequently, we analyzed the research methodologies employed in these papers, extracting critical information such as application type, NN type and architecture, datasets used, training methods, number of NN parameters and operations, memory footprint, quantization approach, development platform, accelerator architecture, and implementation working frequency.

Finally, we reviewed reported results to extract NN application accuracy and other performance metrics, including FPGA resource consumption, NN inference time, FPS, operations per second, power consumption, energy consumption per inference, and operations per second per watt. The data collected from this literature review was organized into a table annexed to this work, facilitating access for readers interested in specific research areas. Python scripts were developed to analyze the gathered data and derive conclusions.

Listing 1. String used to search in the Web of Science

```
(( "fpga*" OR "field-programmable gate array*" OR "field programmable gate array*" OR "programmable logic") AND ("ai" OR "mlp" OR "cnn" OR "perceptron" OR "deep learning" OR "deep-learning" OR "spiking network*" OR "neuromorphic" OR "Neur* Network*" OR "machine learning" OR "ML" OR "artificial intelligence") AND ("spacecraft*" OR "space mission*" OR "satellite*" OR "space app*" OR "cubesat*"))
```

3.1 Real-time runway detection in satellite images using multi-channel PCNN

Zhuang and Low (2014) [187] proposed an FPGA-based implementation of an enhanced pulse-coupled neural network (PCNN) for airfield runway detection in 400x400 RGB images onboard satellites. Unlike other PCNNs, the authors employed a neuron coupling mechanism utilizing feature vectors. This enhanced PCNN performed image segmentation, and its output was filtered using the Hough transform to detect runway features. This FPGA used was a Spartan 3A.

They compared the performance said PCNN with that of the conventional seeded region growing (SRG) method [153]. This comparison reveals that the proposed method outperforms the conventional method by two or three orders of magnitude, depending on the number of segments processed. Furthermore, when detecting runways, this implementation achieved a true positive rate of 88% and a true negative rate of 90%.

3.2 FPGA Architecture for Deep Learning and its application to Planetary Robotics

Gankidi and Thangavelautham (2017) [48] developed a DNN incorporating Q-learning on an FPGA to enhance spacecraft autonomy and decision-making capabilities. This implementation was conducted on a Virtex-7 FPGA, utilizing two distinct approaches. The first method employed a single neuron accelerator, while the second utilized a multilayer perceptron (MLP) accelerator. Both methods leveraged floating-point and fixed-point arithmetic operations to optimize computational efficiency and minimize power consumption. However, this optimization came at the expense of accuracy. This impact was evaluated in two distinct scenarios, comparing both architectures under varying conditions. The MLP accelerator was implemented with 11 neurons for the simplest scenario and 25 neurons for the most complex scenario.

The experimental results demonstrate significant speed improvements. The single-neuron accelerator achieves up to a 95-fold acceleration relative to a conventional Intel i5 CPU. Similarly, the MLP accelerator yields a maximum of 43-fold improvement in processing efficiency compared to this CPU. Furthermore, with respect to power consumption, this latter implementation exhibits a minimum of 5.6 W using fixed-point arithmetic for the simplest scenario and a maximum of 9.7 W using floating-point arithmetic for the more complex scenario.

3.3 FPGA Based Implementation of Convolutional Neural Network for Hyperspectral Classification

Chen et al. (2018) [22] proposed an FPGA-based CNN accelerator for classifying pixels in hyperspectral images into pre-defined categories of ground materials. This accelerator performs inference only, with the CNN model trained offline on GPUs. The design incorporates a pipeline architecture comprising convolution, batch normalization, and dense layers, optimized for efficiency on the FPGA. On-chip ROM storage is employed to store layer parameters, facilitating faster memory access. Furthermore, the Pavia University dataset was used to train and test this system.

The authors report that the FPGA-based CNN implementation yields comparable accuracy results to those obtained using GPUs. Specifically, the system achieved an overall accuracy of 94.58% and an average accuracy of 92.24% in classifying nine classes. Furthermore, the processing speed increased with the utilization of FPGA logic resources, reaching up to 999 pixels per second (or 208 seconds per image) at a clock frequency of 200 MHz.

3.4 An Exploration of FPGA based Multilayer Perceptron using Residue Number System for Space Applications

Jain et al. (2018) [71] proposed a multi-layer perceptron (MLP) FPGA-based accelerator for onboard payload data processing that leverages the Residue Number System (RNS) for number representation. The authors claim that this representation requires fewer hardware resources while yielding equivalent results compared to conventional approaches. This system was tested on the Spartan-6 FPGA using the Crowdsourced Mapping Dataset [76, 77] at a clock frequency of 100 MHz.

The results demonstrate that the system's power consumption was 3.1 W, accuracy was 82.46%, and latency was 7.81 μ s. Notably, compared to an Intel i7 6700HQ CPU, which achieved an accuracy of 86.80% and a latency of 3.67 μ s when running the same NN, this system exhibited higher energy efficiency without significantly compromising performance.

3.5 Ship Classification from SAR Images Based on Deep Learning

Hashimoto et al. (2018) [61] proposed a ship detection and classification method utilizing CNN models for maritime/sea-only scenes. These models were trained and evaluated on Synthetic Aperture Radar (SAR) images acquired from the Phased Array type L-band Synthetic Aperture Radar (PALSAR-2) onboard the Advanced Land Observing Satellite (ALOS-2). Initially, this system was developed to operate on GPUs, and later, an implementation for FPGAs was developed. This FPGA-based implementation leveraged

FINN [163] to generate a CNN accelerator. Both implementations were tested using 36 SAR images containing 513 ships.

The experimental results demonstrate that the GPU-based implementation achieved an accuracy of 99.8% in detecting ships and 65.7% for type classification, with a corresponding average error margin of 26% for ship length classification. In contrast, the FPGA-based implementation successfully detected all 513 ships, achieving 100% accuracy on this test dataset. Notably, the processing time for a single image in the FPGA-based implementation was 330 milliseconds, outperforming GPU and CPU implementations that took 1165 and 7381 milliseconds, respectively.

3.6 Efficient Convolutional Neural Network Weight Compression for Space Data Classification on Multi-fpga Platforms

Pitsis et al. (2019) [138] proposed an FPGA-based CNN accelerator for computing data obtained in deep space onboard a satellite. This accelerator was implemented on the Quad-FPGA Daughter Board (QFDB), which features four Xilinx Zynq Ultrascale+ FPGAs and is utilized in the ESA Euclid deep space mission [143, 119]. Several compression methods were employed to reduce this accelerator memory footprint and successfully implement it in the FPGA. These methods included weight pruning, quantization, and weight clustering, which reduced model size from 173 MB to 11 MB, representing a factor of x16 compression.

A dataset comprising estimated data measurements corresponding to continuous redshifts [157] was created to train and evaluate said system. Experimental results shows that the system computes 4334 signals per second while consuming a maximum of 109 Joules. Compared to the performance of an Nvidia Quadro P1000 GPU, two QFDBs in parallel achieve a throughput that is 1.23 times better, consume 5 times less energy, and exhibit one order of magnitude lower latency. Furthermore, the system reached 416 GFLOPS/s, with a classification accuracy of 99%.

3.7 Artificial Intelligence Implementation on Voice Command and Sensor Anomaly Detection for Enhancing Human Habitation in Space Mission

Kesuma et al. (2019) [81] propose the implementation of an AI Kit capable of detecting faults in the system and receiving commands from the astronauts. This kit implements electronic circuits capable of preprocessing the data retrieved from a microphone and various sensors onboard a spacecraft before sending it to the central computer for processing. This AI Kit communicates with the primary computer system through a UART interface. This computer system constitutes a LEON3 processor implemented on a VIRTEX-5QV FPGA [162], a radiation-hardened FPGA, and it runs a feed-forward NN on the RTEMS 4.1 operating system.

The authors trained and classified the ANN application's performance in detecting three distinct voice commands and anomalies in sensor data. The results demonstrate that this system can accurately classify the voice commands with 99.47% accuracy in 31.74 milliseconds after being trained for 97.90 seconds. The system was capable of achieving 83.3% anomaly detection accuracy after being trained for 28.47 seconds and had an inference time of 14.32 milliseconds.

3.8 A Lightweight Hyperspectral Image Anomaly Detector for Real-Time Mission

Ma et al. (2019) [111] proposed an FPGA-based Pruning-Quantization-Anomaly Detector (P-Q-AD) for hyperspectral images (HSI), which leverages network pruning and quantization within an autoencoder NN. Four implementations were developed to evaluate the performance of P-Q-AD: one utilizing floating-point arithmetic, another incorporating floating-point arithmetic with weight pruning, a third employing 32-bit fixed-weight quantization and pruning, and a fourth featuring custom weight quantization and pruning. The latter quantization approach was determined by solving a multi-objective optimization problem. These implementations were executed on a Zynq UltraScale+ FPGA and compared against Local Reed-XiaoliZ [146] and collaborative representation-based detectors [105] running on two Intel Xeon CPUs.

Three datasets were used to train and evaluate all these implementations: HSI images from Louisiana, San Diego airport in California, and Los Angeles in the USA, acquired by the Airborne Visible Infrared Imaging Spectrometer (AVIRIS) [59]. The results demonstrated that P-Q-AD outperformed traditional approaches by two orders of magnitude and floating-point precision implementations by one order of magnitude while maintaining an area under the curve (AUC) value difference smaller than 0.01. Specifically, this implementation yielded AUC values of 0.9973, 0.9483, and 0.9869 for the Louisiana, San Diego, and Los Angeles dataset s.

3.9 ReCoN: A Reconfigurable CNN Acceleration Framework for Hybrid Semantic Segmentation on Hybrid SoCs for Space Applications

Sabogal et al. (2019) [149] proposed Reconfigurable ConvNet (RECON), a reconfigurable CNN accelerator designed to perform onboard semantic segmentation using a convolutional encoder-decoder NN based on the SegNet model [9]. This accelerator leverages the Hybrid Adaptive Reconfigurable Fault Tolerance (HARFT) [170] framework, which ensures fault tolerance through configuration memory scrubbing and TMR. Prior to synthesis, this accelerator's quantization approach and level of parallelism can be configured. The system was trained and tested using the Potsdam dataset [141] on Xilinx Zynq SoC and Xilinx Zynq UltraScale+ MPSoC platforms. Its resilience to SEUs was assessed through fault injection and neutron radiation tests.

Experimental results revealed significant variability in inference times, power consumption, and FPGA resource utilization as a function of quantization and parallelism employed during testing. Notably, the fastest inference time was 0.7 seconds on the UltraScale+ MPSoC using Q9.18 fixed-point representation, which yielded an accuracy of 88.01% and a power consumption of 25.3 W (21.6 W idle-power + 3.7 W dynamic-power). Conversely, the lowest power consumption was 8.73 W (7.13 W idle-power + 1.60 W dynamic-power) on the Zynq SoC using Q9.16 fixed-point representation, which resulted in an accuracy of 88.00% and an inference time of 4.6 seconds.

3.10 The Insect Brain as a Model System for Low Power Electronics and Edge Processing Applications

Yanguas-Gil et al. (2019) [177] proposed a NN architecture with dynamic learning mechanisms inspired by the insect brain's mushroom body [8]. This architecture targets resource-constrained environments, such as space exploration, and was implemented in both FPGA-based non-spiking and spiking configurations using the Loihi neuromorphic chip [35]. The FPGA-based implementation followed the ModNet architecture [34] and incorporated a modulatory component to enable online supervised training on the MNIST dataset. To optimize resource utilization, fixed-point arithmetic and operation folding techniques were employed.

The results of these implementations demonstrated that the accuracy obtained using the FPGA-based configuration was comparable to that achieved by the Loihi neuromorphic chip. Specifically, after training with 1000 images, an accuracy of 80% was attained, while training with 20,000 images resulted in an accuracy of 91%. Furthermore, the FPGA implementation demonstrated fast training times, achieving convergence within under 20 seconds, and low power consumption of only 1W.

3.11 Towards an Efficient Accelerator for DNN-Based Remote Sensing Image Segmentation on FPGAs

Liu and Luk (2019) [107] proposed a CNN accelerator for remote sensing image segmentation, integrating convolutional and deconvolutional layers within a single module. This design leverages parallelism through multiple channels and filters inherent to these layers, thereby enhancing computational efficiency. Several optimizations were incorporated into its design, including 8-bit quantization, layer fusion, input reshaping, and tailored DSP configuration.

The proposed system was evaluated using urban surface images of 256x256 pixels on an Arria 10 SX SoC, utilizing a modified U-Net model NN as the test case. The results demonstrated that the proposed U-Net achieved an accuracy of 80.1%, with an inference time of 17.4 ms and a throughput of 1578 GOPs per second. Furthermore, the total power consumption of this system executed on the development board was measured to be 32 W.

3.12 Efficient Object Detection Framework and Hardware Architecture for Remote Sensing Images

Li et al. (2019) [104] proposed a Context-Based Feature Fusion Single-Shot multi-box Detector (CBFF-SSD) algorithm, which was implemented on a Zynq 7000 FPGA for object detection in high-resolution images onboard satellites. Building upon the SSD NN architecture [108], the CBFF-SSD algorithm leveraged MobileNet [67] as its backbone network to enhance efficiency. The Deep Learning Processor (DLP) developed for this implementation consists of a Neural Processing Engine (NPE), control modules, and memory buffers. The NPE is an array of Neural Processing Units (NPU), where each NPU contains a matrix of PEs. The NWPU VHR-10 dataset [23, 25] was used to fine-tune a pre-trained model trained on the VOC0712 [44] dataset and evaluate the system's performance.

Experimental results demonstrated that this algorithm achieved a mean average precision of 91.42%. The DLP consumed 19.52 W of power, which was 29.74 and 2.87 times more efficient than a Intel i7-7700 CPU and NVIDIA GeForce GTX1070T GPU respectively. Notably, while not outperforming other FPGA-based accelerators in raw performance, this architecture achieved the highest performance density, 1.97 OP/DSP/cycle.

3.13 Low-Power Neural Networks for Semantic Segmentation of Satellite Images

Bahl et al. (2019) [10] proposed several compact NN architectures, namely C-UNet/C-UNet++ and C-FCN/C-FCN++, for semantic segmentation on low-power devices. These networks were trained and evaluated for two use cases: cloud and forest segmentation. The datasets utilized for these use cases were the Cloud-38 [123] and CloudPeru2 datasets [125] for cloud segmentation and the EOLearn Slovenia 2017 dataset [37] for forest segmentation. Inference was performed on a Raspberry Pi platform, and the C-FCN++ architecture was implemented on a Cyclone V FPGA.

The smallest model presented was the C-FCN++, with only 273 parameters, occupying 0.047 MB. In contrast, the largest model developed was the C-UNet, with 51,113 parameters, occupying 0.735 MB. Notably, the performance of these models differed significantly. The C-UNet demonstrated comparable accuracy, precision, and recall to the U-Net model. Conversely, the C-FCN++ exhibited an accuracy decay of 2.55%, 5.05%, and 5.93% for the Cloud-38, CloudPeru2, and EOLearn Slovenia 2017 datasets compared to the C-UNet. This model's FPGA implementation enabled real-time analysis of images captured by the OPS-SAT's camera, with cloud segmentation performed on a 2048x1944 image in less than 150 milliseconds.

3.14 FPGA acceleration of a quantized neural network for remote-sensed cloud detection

Reiter et al. (2020) [147] proposed a BNN accelerator for cloud detection, leveraging a characteristic quantization method where both weight and activation values are quantized to binary levels (1-bit). This BNN architecture was based on the CNV-W1A1 model in the Brevitas libraries [135] and implemented on the Artix-7 FPGA using FINN [163]. The training and testing datasets employed were a custom ESA Copernicus Sentinel-2 dataset [37] and the Planet dataset [155], with TMR being discussed as a potential method to mitigate SEU effects. However, its implementation was hindered due to limited FPGA memory resources.

When executed on the FPGA, the NN model's performance was found to be suboptimal compared to its execution without quantization on both CPU and GPU. Specifically, the inference accuracy on the FPGA was 64%, whereas it reached 91.8% on the CPU and 91.9% on the GPU. Despite the relatively low accuracy, the experiment revealed that the BNN model on the FPGA exhibited a power consumption of 2.4 W, a runtime of 2.8 milliseconds, and a throughput of 358.1 images per second. In comparison to the Nvidia Tesla M60 GPU, the FPGA demonstrated a significant advantage in terms of speed (7.9 times faster) and energy efficiency (120 times less power).

3.15 An FPGA-Based Hybrid Neural Network Accelerator for Embedded Satellite Image Classification

Lemaire et al. (2020) [94] proposed an FPGA-based accelerator for a Hybrid Neural Network (HNN) designed for cloud detection onboard satellites, leveraging the LeNet model [93] as its foundation. This HNN integrates a traditional CNN with an SNN architecture. Its accelerator comprises three primary components: the feature extraction module, which is implemented following a traditional CNN approach inspired by previous work [57]; the interface between the traditional CNN and SNN component, which converts rate-based data into spike trains; and the classification SNN layers, in which each neuron follows the Integrate and Fire (IF) model [17].

This system was successfully implemented at a clock frequency of 100 MHz on a Cyclone-V FPGA, mirroring the hardware configuration employed by the OPS-SAT [42, 43]. The implementation yielded an accuracy of 87%, latency of 43 μ s, logic cell occupation of 59%, and power consumption of 1192.66 mW. In contrast, its counterpart, implemented without incorporating SNN components, achieved an accuracy of 88%, latency of 25 μ s, logic cell occupation of 71%, and power consumption of 1248.44 mW.

3.16 Evaluating the Cognitive Network Controller with an SNN on FPGA

Lent (2020) [97] proposed an implementation of the Cognitive Network Controller (CNC) [95] on an FPGA to address routing challenges in Delay-tolerant networking (DTN) [96] onboard satellites. This

implementation leveraged an SNN to decide upon outbound connections and store information regarding its decision-making performance. The CNC employs an SNN with STDP, meaning it can be applied to new scenarios without prior training, and over time, it will adapt and become more proficient. The SNN architecture in this CNC utilized a Leaky-Integrate-and-Fire (LIF) neuron model and was implemented on a Zynq 7020 System-on-Chip (SoC) with 256 neurons. Additionally, this implementation was tested on a 5-node network testbed.

The results demonstrated the advantage of this implementation compared to a CPU-only solution, showing a lower response time and higher throughput than Contact Graph Routing (CGR), which served as a reference. Notably, leveraging the FPGA fabric to accelerate the CNC SNN inference, this system executes the SNN inference 32 times faster than its software-only counterpart.

3.17 Utilization of FPGA for Onboard Inference of Landmark Localization in CNN-Based Spacecraft Pose Estimation

Cosmas and Kenichi (2020) [29] presented an FPGA-based CNN accelerator for spacecraft pose estimation, leveraging Vitis AI on an Ultra96v2 board featuring an UltraScale+ MPSoC. Their implementation had three primary stages: spacecraft detection, image cropping, and heatmap-based key points detection. YOLOv3 [145] was employed for spacecraft detection and image cropping, with the resultant output being resized to 128x128 pixels before input into a ResNet34-U-Net model for key points detection. Utilizing Vitis AI, these networks were optimized through pruning and quantization. These networks were evaluated on three distinct Xilinx DPU IP [4] architectures; however, due to hardware constraints, only one instance of these DPUs was implemented on the FPGA. The proposed system was trained and evaluated using the SPEED dataset [85].

The results demonstrate an RMS error difference between the FPGA and PC implementations smaller than 0.55, with an average RMS error of 1.913 for the FPGA and 1.382 for the PC over 100 images. Notably, the FPGA implementation exhibited on-chip power consumption ranging from 3.4 to 3.9 W, while the board consumed 8.6 W during inference.

3.18 FPGA Implementation for CNN-Based Optical Remote Sensing Object Detection

Zhang et al. (2021) [183] proposed a hardware implementation of an improved YOLOv2 network on a Zynq 7000 SoC for optical remote-sensing object detection. This hardware leveraged multiple parallel PEs to achieve efficient computation, and the PEs utilizes model quantization and layer fusion, supporting various convolution types. The proposed quantization technique employs an 8-bit fixed-point representation for feature maps and weights, whereas biases and the output of convolutional layers are represented using 32-bit fixed-point arithmetic. In contrast, batch normalization and activation layers use 32-bit floating-point representations. This system was implemented with 32 PEs, and the DOTA dataset [172] was used to train and test it.

The experimental results demonstrate that this FPGA implementation achieved an inference time of 3.4 seconds with a power consumption of 5.96 watts, showcasing significant energy efficiency gains compared to the CPU. Specifically, this implementation is 33.4 times more energy efficient than its CPU counterpart. Notably, despite the GPU implementation outperforming in throughput (47.3 times faster), this FPGA implementation achieves only 2.384% of the GPU's power consumption. Furthermore, this performance was obtained at a marginal cost to mean average precision (mAP), with only a 0.18% decrease compared to GPU implementations.

3.19 An FPGA-Based Hardware Accelerator for CNNs Inference on Board Satellites: Benchmarking with Myriad 2-Based Solution for the CloudScout Case Study

Rapuano et al. (2021) [144] proposed an FPGA-based CNN accelerator for cloud detection onboard satellites, leveraging a modified variant of the CloudScout [53] model. This variant was optimized through custom fixed-point arithmetic, resulting in a 48% reduction in memory footprint, from 204 to 107 Mbits, with a negligible accuracy drop of 0.3%. The accelerator's hardware design incorporated a custom cache system, a shared convolutional PE, an on-chip filter ROM, a max pooling PE, and a FC PE. This accelerator was implemented on a Zynq Ultrascale+ ZCU106 development board and synthesized for a Radiation Tolerant (RT) Kintex UltraScale XQRKU060 FPGA.

Results demonstrated that on the Zynq board, the inference time was 141.68 milliseconds, and the power consumption was 3.4 watts. In contrast, the estimated inference time on the Kintex FPGA was 264.72 milliseconds, with an estimated power consumption of 1.6 watts. Notably, the FPGAs

utilized in this study exhibited superior energy efficiency compared to the CloudScout Myriad 2 [127] implementation. The Zynq board's energy efficiency was 0.48 J, whereas that of Myriad 2 was 0.63 J. Furthermore, Myriad 2 exhibited an inference time of 346 milliseconds and a power consumption of 1.8 W.

3.20 Reconfigurable Framework for Resilient Semantic Segmentation for Space Applications

Sabogal et al. (2021) [150] enhanced their previous work [149] by refining RECON, an on-board semantic segmentation accelerator. This accelerator was evaluated using the SegNet model [9], trained on the Potsdam dataset [141]. To mitigate SEEs, its design incorporated TMR and configuration memory scrubbing. Furthermore, this design included several optimizations such as 8-bit quantization, feature map caching, Winograd transform, batch normalization, layer folding, layer fusion, and operating DSPs at twice the frequency of surrounding logic. This accelerator's configuration parameters, NN weights, and TMR usage could be dynamically configured at runtime. Consequently, various configurations were tested on the Zynq 7020 SoC and the Zynq UltraScale MPSoC to assess performance and dependability. Its dependability was evaluated through configuration memory fault injection and neutron irradiation to quantify SEE susceptibility.

Results from these tests demonstrated that executing the same algorithm on RECON yielded a power efficiency improvement of two orders of magnitude compared to CPU execution on the board. The 8-bit quantization approach resulted in a degradation of 1.68% or less in mean intersection-over-union and 1.33% or less in F1 accuracy metrics values. Notably, when comparing configurations with and without TMR, the TMR-enabled configuration exhibited a significant 56-fold reduction in vulnerability to application hanging due to SEEs despite increased FPGA resource utilization, lower performance, and reduced power efficiency.

3.21 A Multi-Cache System for On-Chip Memory Optimization in FPGA-Based CNN Accelerators

Pacini et al. (2021) [133] proposed an FPGA-based CNN accelerator with optimized memory usage for cloud detection onboard satellites, building upon the previously developed accelerator [144] for the CloudScout [53] model. The accelerator improvements are centered around an L1 Cache and a Filter Cache system. The L1 Cache system is designed to reuse data from the input filter maps, thereby reducing the size of the input feature maps buffer, which is subsequently alleviated by the L2 Cache system. In contrast, the Filter Cache plays a crucial role in storing the filters of a single layer on-chip, thereby augmenting the accelerator's efficiency.

This accelerator was successfully implemented across various FPGAs, including ZU3EG, Z7030, XC7A200T, KU025, and A10 GX 270, demonstrating its adaptability. The results obtained from implementing this accelerator on the Zynq Ultrascale+ XCZU7EV MPSoC reveal improved on-chip memory utilization while maintaining comparable accuracy, performance, and power consumption. Specifically, this accelerator achieved inference in 144.8 ms and consumed 4.51 W. Notably, compared to the Intel Movidius chip, this implementation exhibits higher power consumption and lower inference time.

3.22 Algorithm/Hardware Codesign for Real-Time On-Satellite CNN-Based Ship Detection in SAR Imagery

Yang et al. (2022) [175] proposed OSCAR-RT, an algorithm/hardware co-design framework for CNN-based SAR ship detection onboard satellites. This framework receives the targeted accuracy, latency, and FPGA as input and outputs a set of possible CNN architectures along with their corresponding hardware implementations. This hardware is generated using pre-built HLS-based CNN components. The authors employed filter pruning and mixed-precision quantization techniques to make these architectures suitable for onboard computing. Moreover, this framework was evaluated by generating six CNN accelerators based on the MobileNetV1 [67], MobileNetV2 [151], and SqueezeNet [69] models, trained with the SSDD dataset [101]. These accelerators were implemented on a Virtex 7 FPGA VC709 Connectivity Kit featuring an XC7VX690T FPGA.

Experimental results demonstrated that the accelerators generated with OSCAR-RT achieved an average precision of between 93.3% and 94.6% while ensuring high performance and minimizing power consumption. These accelerators achieved up to 366 GOP/s and consumed as little as 4.4 Watts. Notably, compared to the Nvidia RTX 2080Ti GPU running the same models, OSCAR-RT obtained significantly

improved performance metrics, including a latency reduction of up to 2.4 times with the MobileNetV2 model and a power consumption decrease of up to 11.6 times.

3.23 Resources and Power Efficient FPGA Accelerators for Real-Time Image Classification

Kyriakos et al. (2022) [90] proposed an FPGA-based CNN accelerator for ship detection. This CNN was designed as a lightweight model tailored for on-board computing, comprising two convolutional layers, two pooling layers, and one FC layer. This accelerator leveraged fixed-point arithmetic within its computational units, representing values within the NN with 8 to 17 bits of precision. Its design was implemented using reusable VHDL blocks developed by the authors and evaluated on the Virtex 7 FPGA VC707 Evaluation Kit. The CNN model was trained on the Planet’s “Ships in Satellite Imagery” dataset [60].

The experimental results demonstrated that this lightweight model achieved an accuracy of 97.6% in detecting ships. Notably, this accelerator enabled concurrent inference of two frames (80x80 RGB image), requiring only 0.687 ms to process a single frame. When compared with CPU and GPU execution, this accelerator exhibited speedups of 6.836 and 3.205, respectively. Compared to the Jetson Nano and Myriad 2 devices, this accelerator outperformed them in terms of performance. However, these devices demonstrated higher performance per watt.

3.24 FPGA-Based Implementation of a CNN Architecture for the On-Board Processing of Very High-Resolution Remote Sensing Images

Neris et al. (2022) [128] proposed a CNN accelerator for a lightweight version of the MobileNetv1 model [67], designed to detect ships and airplanes on images obtained through sensors within the Video Imaging Demonstrator for Earth Observation (VIDEO) project [28]. The NN was trained using ship and airplane datasets to accomplish this task. These datasets consisted of a combination of the MASATI dataset [47] and a subset of the HRSC2016 dataset [110], comprising 512x512 RGB images, as well as the UC Merced Land Use dataset [176] and the Aerial Image dataset [173], containing 256x256 RGB images. Two distinct implementations of this accelerator were realized on a Kintex Ultrascale FPGA using Vitis HLS. One implementation utilized 32-bit floating-point arithmetic, while the other employed 16-bit fixed-point arithmetic.

Experiments revealed that the MobileNetv1Lite model executes approximately 0.05 GFLOPs for ship detection and 0.012 GFLOPs for aircraft detection. Furthermore, the $F1_{Score}$ achieved for these tasks was approximately 94.5% and 91%, respectively. Notably, the quantization approach adopted led to a reduction in the number of LUTs, FFs, and block RAMs (BRAMs) required when implementing on hardware, while also taking better advantage of the available DSP units.

3.25 Automatic Deployment of Convolutional Neural Networks on FPGA for Spaceborne Remote Sensing Application

Yan et al. (2022) [174] proposed a CNN accelerator comprised of multiple parallel PEs that can be dynamically configured at runtime to execute distinct network layers. This capability is achieved by compiling a PyTorch model into instructions and loading them onto the FPGA. These PEs also leverage several optimizations, including quantization, which resembles a previous work [183], unified layer operations, convolution dataflow rearrangement, and dynamic slicing of input feature maps. This accelerator was evaluated on an Artix 7 FPGA with eight PEs with an improved VGG16 model for scene classification on the NWPU-RESISC45 dataset [24] and an improved YOLOv2 model for object detection on the DOTA-v1.0 dataset [172].

The results demonstrated that the developed accelerator achieved an inference time of 1.78 seconds for the VGG16 experiment and 17.12 seconds for the YOLOv2 experiment, consuming only 3.407 watts. In contrast, the Intel Xeon Gold 5120T CPU and an Nvidia Titan Xp GPU consumed 31 times and 73 times more power than this accelerator. Furthermore, compared to these platforms, there was a decrease of 0.05% in overall accuracy for the VGG16 experiment and 0.2% in mean average precision for the YOLOv2 experiment.

3.26 CloudSatNet-1: FPGA-Based Hardware-Accelerated Quantized CNN for Satellite On-Board Cloud Coverage Classification

Pitonak et al. (2022) [137] proposed CloudSatNet-1, an FPGA-based CNN accelerator to reduce the amount of downlinked data from CubeSats by performing onboard cloud detection. This accelerator was implemented on the Zturn board, which contains a Zynq Z7020 SoC, by leveraging the FINN framework [163, 14]. The framework enabled testing nine different configurations with varying quantization approaches (2-, 3-, and 4-bit width parameters) and levels of parallelism. The CloudSatNet-1 model was trained and tested using the Landsat 8 Cloud Cover Assessment Validation data (L8 biome dataset) [45] to evaluate the impact of these configurations on the False Positive Rate (FPR) and accuracy.

The results demonstrated that excluding Snow/Ice biomes from the training data improved accuracy ($ACC \approx 92\text{-}95\%$) and reduced FPR ($\approx 2.9\text{-}5.7\%$) compared to training with the full dataset ($ACC \approx 88\text{-}90\%$, $FPR \approx 7\text{-}10\%$). Notably, increased parameter width resulted in higher accuracy and lower FPR values. Furthermore, the results showed that accelerators with varying levels of parallelism achieved distinct performance metrics: an accelerator without parallelism reached 0.9 FPS. In contrast, the accelerator with maximum layer parallelization achieved 15 FPS. The power consumption of these accelerators varied between 2.448 W and 2.592 W, respectively.

3.27 Accurate, Low-latency, Efficient SAR Automatic Target Recognition on FPGA

Zhang et al. (2022) [182] proposed a Graph Neural Network (GNN) model and an FPGA-based accelerator for it. This accelerator was designed for the Zynq UltraScale+ MPSoC ZU7EV and leveraged optimizations, such as weight and input pruning. These optimizations reduced the model's memory footprint and computational requirements. Compared to a previous work CNN model [6], this GNN model computation complexity was $\frac{1}{3258}$, and it contained $\frac{1}{83}$ parameters on average, thereby requiring significantly less memory. This GNN model comprises GNN layers (GNNL) with GraphSAGE layer operators [58], graph pooling layers, and Attention modules.

Additionally, this accelerator was tested using the MSTAR dataset [156], where each SAR image has a size of 128x128 pixels. When executed at 125 MHz, the testing results demonstrated an inference time of 0.105 milliseconds and a power consumption of 6.3 W, with an accuracy of 99.09%. Compared to CPU and GPU implementations, these results represented a speedup of 14.8x and 2.5x and an improved energy efficiency of 62x and 39x, respectively.

3.28 SPLEAT: SPIking Low-power Event-based ArchiTecture for in-orbit processing of satellite imagery

Abderrahmane et al. (2022) [1] proposed SPLEAT, an FPGA-based SNN accelerator designed for cloud detection onboard the OPS-SAT satellite equipped with a Cyclone V FPGA [42, 43]. The authors implemented two distinct architectures of SPLEAT: one utilizing serial spike generation and the other employing parallelization. These implementations were compared with a CNN and a Hybrid NN (HNN) implementation regarding inference time and power consumption. These networks were based on the LeNet model and trained and tested using the OPS-SAT cloud dataset. The HNN utilized conventional convolutional layers followed by spiking dense layers.

The results indicated that the estimated inference time for the CNN was 25 μs ; for the HNN, it was 280 μs ; for the SNN utilizing serial spike generation, it was 1860 μs ; and for the SNN employing parallel spike generation, it was 160 μs . In terms of power consumption, the accelerator's usage for the CNN was 243.99 mW; for the HNN, it was 295.99 mW; for the SNN with serial spike generation, it was 41.28 mW; and for the SNN with parallel spike generation, it was 201.69 mW. Notably, among the four tested ANN architectures, the SNN with serial spike generation achieved the highest accuracy of 71.92% on the provided dataset.

3.29 Hardware Acceleration and Implementation of YOLOX-s for On-Orbit FPGA

Wang et al. (2022) [167] proposed an FPGA-based accelerator for the YOLOX-s model [51], a CNN designed for object detection tasks that has been trained on the COCO dataset [106]. Said accelerator design leveraged a DSP array for convolutional layer computation and a cache system to store feature maps and weights efficiently. Notably, during design and experimentation, the authors accounted for the hardware implications of TMR, utilizing one-third of the available DSPs to reserve resources for future radiation-tolerant implementations.

The experimental results were obtained by implementing this accelerator on an FPGA within the Virtex 7 FPGA VC709 Connectivity Kit. These results demonstrated an FPGA power consumption of 14.76 W, an inference time of 62.187 ms, and a throughput of 399.6 GOP/s. Additionally, the authors reported a DSP utilization rate of 85.33% during inference, indicating efficient computation and reduced dependence on memory bandwidth.

3.30 SoC FPGA Acceleration for Semantic Segmentation of Clouds in Satellite Images

Papatheofanous et al. (2022) [134] proposed the Lightweight Dilation UNet (LD-UNet), a compact model for semantic segmentation tasks. This NN was implemented on a Zynq UltraScale+ MPSoC and trained on the 95-Cloud dataset [124] for cloud detection. The implementation relied on Vitis AI [165] and HLS to generate the hardware design for the FPGA. Furthermore, Vitis AI employed quantization techniques to utilize an 8-bit fixed-point arithmetic, achieving a higher performance.

The results indicated that the quantization approach led to a small degradation in accuracy, Intersection over Union (IoU), recall, and precision. Notably, when utilizing the FPGA as an accelerator, this application demonstrated a speedup of 1.64. According to the Vivado power analysis report, the accelerator exhibited a power consumption of 14.111 W.

3.31 RF Fingerprinting Identification Based on Spiking Neural Network for LEO-MIMO Systems

Jiang and Sha (2023) [74] proposed an FPGA-based radio frequency fingerprinting identification method leveraging SNNs. This method employed an SNN based on the leaky integrate-and-fire (LIF) model, which was trained using Spatiotemporal backpropagation (STBP) [171]. This NN was implemented on a Virtex 7 FPGA and trained on a dataset comprised of 56,000 MATLAB simulation samples obtained at different signal-to-noise ratios (SNRs).

The experimental results demonstrated that at an SNR of 25dB, the model achieved an accuracy of 95.26%, inferred an image in 27.14 ms, and consumed 1.78 watts.

3.32 Evaluation of Xilinx Versal Architecture for Next-Gen Edge Computing in Space

Perryman et al. (2023) [136] analyzed the performance of AMD/Xilinx Versal Adaptive Compute Acceleration Platform (ACAP) [132] for computing several space-domain-specific applications. These applications included three NNs (MobileNetV1 [67], ResNet-50 [62], and GoogLeNet [160]) and a communication-based application, which were implemented on different components of this platform: the ARM Cortex-R5F CPU, the ARM Cortex-A72 CPU, the FPGA fabric, and the AI engines. Each of these implementation was compared regarding computing speed, power consumption, and FPGA fabric resource consumption. Furthermore, the performance of these implementations was further compared to the same applications run on the Xilinx Zynq 7-series SoC.

This analysis demonstrated that the Versal FPGA fabric achieves the highest computing speed while being the most power-consuming implementation. When executing the NN applications, the implementation using the Versal FPGA achieved a 36.73x speedup over its ARM Cortex-R5F CPU counterpart while consuming 33.04 W. Regarding resource utilization, the Versal AI engines implementation almost entirely avoids utilizing FPGA fabric resources, and the FPGA fabric implementation uses only a little percentage of available resources. Furthermore, the results obtained from the Zynq 7-series SoC implementations are identical to those achieved on the Versal platform.

3.33 Resource-constrained FPGA Design for Satellite Component Feature Extraction

Ekblad et al. (2023) [40] implemented a YOLOv4-based NN model on an FPGA utilizing Vitis AI for satellite component detection. This model deviated from the original YOLOv4 [16] to accommodate Vitis AI. Specifically, the Mish activation function [121] was replaced with leaky ReLU [112], and the max pooling kernel size was reduced to 8x8. Furthermore, the model was quantized to an 8-bit fixed-point representation using Vitis AI. This implementation was evaluated on the Kria KV260 Vision AI Starter Kit, which features a Zynq UltraScale+ MPSoC. The dataset employed for this evaluation consisted of images captured at the Florida Institute of Technology's ORION facility utilizing the Kinematics Simulator.

The results indicated that the mean Average Precision (mAP) decreased by 2.9% relative to the original model, primarily attributed to the quantization process and FPGA implementation. Notably, this implementation outperformed a previous work [114], where the authors deployed the YOLOv5 model [75] on an Intel NCS2 and Raspberry Pi, achieving 3.8 FPS compared to 2 FPS.

3.34 Systematic Reliability Evaluation of FPGA Implemented CNN Accelerators

Gao et al. (2023) [49] evaluated the susceptibility to SEUs of FPGA-based CNN accelerators designed for onboard spacecraft applications. The accelerators, comprising AMD/Xilinx Deep Learning Processing Units (DPU) [4], were implemented in three versions with varying levels of parallelism. These implementations were deployed on 20 Zynq 7000 SoC devices and tested using the VGG16 [154], ResNet20 [62], and MobilenetV2 [151] models by inducing a single-bit flip in the architecture. The authors analyzed the performance impact of SEUs in the computing engine, data mover, and instruction scheduler components of each accelerator variant for each of these tests.

The results showed that the computing engine and data mover components utilized the most hardware resources on the FPGA. Most of the SEUs that occurred on these components caused accuracy deterioration, with less than 0.2% and 20.31% causing system corruption, respectively. Furthermore, it was found that SEUs causing system corruption predominantly occurred in the data mover and instruction scheduler, whereas SEUs leading to accuracy deterioration primarily occurred in the computing engine. Notably, the reliability of this later component improved with an increase in the level of parallelism.

3.35 AI-Based Real-Time Star Tracker

Carmeli and Ben-Moshe (2023) [18] proposed a Self-Organizing Map (SOM) accelerator for identifying star patterns from images captured by onboard satellite cameras as part of an end-to-end environment that encompasses image capture, processing, and spacecraft position identification. This system leverages a DE1 evaluation board featuring an ARM hard-core processor, a high-sensitivity VIS camera, a display showing the captured image, and a graphical user interface (GUI) application for testing and displaying results. Upon initialization by the ARM processor, the system filters the captured image to remove dead pixels and executes the main algorithm while interfacing with the Cyclone-V FPGA. The latter controls the camera for capturing images, processes them using the SOM NN, and interfaces with the GUI application. The SOM NN receives a feature vector derived from the positions of stars in the image as input and compares it to data stored in the Almanac.

The proposed accelerator enables efficient identification of star patterns while minimizing memory utilization compared to alternative approaches. Notably, the SOM NN executes in approximately 870 microseconds and requires 249 kilobytes of memory with a confidence level of roughly 98% in its ability to accurately identify star patterns.

3.36 FPGA Accelerator for Meta-Recognition Anomaly Detection: Case of Burned Area Detection

Coca and Datcu (2023) [27] implemented the ResNet model [86] on an FPGA to detect natural anomalies, such as wildfires, in multispectral imagery. This model was trained and tested on three datasets: the BigEarthNet [158, 159] and two Sentinel-2 products [50], Zamora and Bordeaux. The model was initially trained on a machine comprising an Intel Xeon CPU and a Tesla K80 GPU and then implemented on a ZCU102 board. This implementation leverages the AMD/Xilinx DPUCZDX8G [4] and quantizes the model's parameters to 8-bit values. The board's CPU processes the input and output of the CNN, and the FPGA executes the CNN architecture.

The results showed that the quantized model exhibited lower precision than the original 32-bit floating point data, with an accuracy of 73.7% in the BigEarthNet dataset, as opposed to 81.1%. However, this implementation demonstrated several advantages over the Tesla K80 GPU, including a reduced inference time of 0.7 seconds versus 3.128 seconds, an increased FPS of 85.677 compared to 19.861, and lower power consumption of 30 W versus 135 W. When compared to other platforms such as the RPi-Movidius system [36] and P-Q-AD [111], this implementation achieved a speed-up of 2.24x and 4.16x respectively, and reduced hardware resource consumption.

3.37 Hardware Acceleration of Satellite Remote Sensing Image Object Detection Based on Channel Pruning

Zhao et al. (2023) [186] proposed a lightweight NN model, YOLOv4-MobileNetv3, for object detection onboard spacecraft. This model was implemented on a Kria KV260 board featuring a Zynq UltraScale+ MPSoc, leveraging AMD/Xilinx's B4096 DPU architecture and Vitis AI. This model was constructed by modifying the original YOLOv4 model [16]. These modifications included adopting MobileNetv3 [66] as the backbone feature extraction network, model channel pruning, and post-training quantization (PTQ).

This later method quantized the parameters from a 32-bit floating-point number into an 8-bit fixed-point number format.

The proposed implementation was evaluated on the DIOR dataset [103]. This evaluation demonstrated a reduction in parameter size of 91.11% compared to the original YOLOv4 model at the cost of 1.86% mean average precision (mAP). Furthermore, compared to an AMD R7-4800H CPU, this implementation reduced power consumption by 81.91% and increased FPS by 317.88%. Similarly, compared to an NVIDIA RTX 2060 GPU, this implementation reduced power consumption by 91.41% and increased FPS by 8.50%.

3.38 Algorithm-Hardware Co-Optimization and Deployment Method for Field-Programmable Gate-Array-Based Convolutional Neural Network Remote Sensing Image Processing

Ni et al. (2023) [130] proposed a CNN accelerator for onboard spacecraft execution, which was implemented on a VC709 board featuring a Virtex-7 FPGA and controlled by an attached Zedboard. This accelerator leverages diverse optimizations to minimize resource and power consumption, including depth-wise mapping techniques and utilizing its PEs to execute multiple layers with similar structures. These optimizations enabled the accelerator to achieve significant reductions in resource utilization. Furthermore, this accelerator was tested by executing the YOLOv2 network [109], trained with the DOTA-v1.0 [172] dataset, for object detection, and the ResNet-34 [62] and VGG-16 networks [154], trained with the NWPU-RESISC45 dataset, for scene classification.

The results showed that the CNN accelerator operating at 200 MHz consumes 14.97 W of power while maintaining an energy efficiency of 12.18 to 25.83 GOP/s/W, depending on the model executed. Notably, this accelerator demonstrated superior energy efficiency compared to other state-of-the-art accelerators [179, 32, 181, 82, 126, 166, 73], the Intel Xeon E5-2697v4 CPU, and the NVIDIA TITAN Xp GPU. The CPU achieved energy efficiencies ranging from 0.37 to 1.47 GOP/s/W, while the GPU yielded values between 2.45 and 23.16 GOP/s/W.

3.39 An Overlay Accelerator of DeepLab CNN for Spacecraft Image Segmentation on FPGA

Guo et al. (2024) [56] proposed an FPGA overlay CNN accelerator for semantic spacecraft component images (SCIs) segmentation. Compared to other existing CNN accelerators for FPGAs, this overlay approach allows the execution of various CNN models without changing the hardware implementation. To achieve this implementation, the authors worked on a COD (Control, Operation, and Data transfer) Instruction Set Architecture (ISA), a compiler for this ISA, and a hardware accelerator design. This overlay was implemented on a Virtex-7 FPGA and tested using six CNN models trained with the Spacecraft Dataset [38] and the SCIs Dataset [55]. These CNN models incorporate a combination of a backbone network (VGG16 [154], ResNet18 [62], or SqueezeNet1.1 [69]) and a head network (DeepLabv3+ [21] or DeepLabv3 [20]).

The results were compared to inference on existing CNN image segmentation accelerators, other FPGA overlay solutions, and an NVIDIA RTX 2080Ti GPU. This implementation demonstrates higher computational resource efficiency than previous image segmentation accelerators and other FPGA overlay solutions, resulting in a performance of 159.48 GOP/s with reduced hardware resources. While not outperforming the GPU, their implementation exhibits a 5.1x improvement in energy efficiency, consuming 21 W, which is crucial for space application.

3.40 Online continual streaming learning for embedded space applications

Mazouz and Nguyen (2024) [117] proposed an FPGA-based NN accelerator incorporating online continuous learning (OCL), a method inspired by experience replay (ER) literature [148]. This method addresses the challenges associated with temporal variations in deployment environments. A custom dataset comprising images from the AARST telescope [164] was utilized to train a YOLOv3 model [145] for object detection. This dataset was divided into old and new categories, enabling experimentation with OCL effectiveness by varying the proportions of new and old data within input batches of variable sizes. This accelerator was implemented on a Zynq 7100 board using their CNN FPGA compiler [116, 115], with training performed via an onboard backpropagation pipeline and the proposed OCL methodology.

The results demonstrated that utilizing 100% of available DSPs and 86% of LUTs in the FPGA enabled a CNN to adapt to new environments using OCL within 3.96 minutes. However, achieving optimal average learning and forgetting values required additional iterations, with the best results obtained

after five iterations (8.40 minutes). The accelerator achieved a processing rate of 90 FPS, theoretically sufficient for real-time benchmarking input processing.

3.41 A Configurable Accelerator for CNN-Based Remote Sensing Object Detection on FPGAs

Shao et al. (2024) [152] proposed an FPGA-based CNN accelerator controlled with microinstructions using a very long instruction word (VLIW) architecture. This accelerator incorporates one or more systolic arrays that leverage the DSP units available on the FPGA. These units efficiently execute multiply-accumulate operations and can compute various CNN layers. Furthermore, this accelerator employs 16- and 8-bit fixed-point data quantization to reduce the storage and computational load. This system was implemented in a Virtex-7 FPGA and evaluated with two distinct configurations: one featuring a single systolic array and 16-bit precision and another comprising two systolic arrays and 8-bit precision. These implementations were tested by executing the YOLOv3-Tiny and ResNet-18 models on the NWPU VHR-10 dataset [13].

For a single-systolic array implementation with 16-bit quantization, the system achieved 51 FPS, 153.14 GOPS/s, and a power consumption of 6.93 W when executing the ResNet-18 model. For a two-systolic array implementation with 8-bit quantization, the system achieved 102 FPS, 301.52 GOPS/s, and a power consumption of 10.68 W when executing the YOLOv3-Tiny model.

3.42 An FPGA-Accelerated CNN with Parallelized Sum Pooling for Onboard Realtime Routing in Dynamic Low-Orbit Satellite Networks

Kim et al. (2024) [83] proposed a dueling DQN-based reinforcement learning algorithm, which was accelerated on a PYNQ-Z2 board leveraging a CPU and an FPGA. This algorithm was specifically designed for real-time routing in LEO satellite networks. A key component of this algorithm is a CNN, which was implemented on the FPGA fabric using HLS. This CNN comprised convolutional and ReLU layers, which were inferred onboard.

The FPGA-based acceleration outperformed CPU execution by a factor of 3.10. Specifically, the average execution time of this implementation was 0.2991 seconds.

3.43 An Energy-Efficient Artefact Detection Accelerator on FPGAs for Hyper-Spectral Satellite Imagery

Castelino et al. (2024) [19] implemented a convolutional autoencoder (CAE) on the ZCU104 board to detect artifacts in Hyper-spectral imaging (HSI) images using Vitis AI [5] and Xilinx B4096 DPU IP core [4]. This CAE was trained and tested on a combined dataset of the Indian Pines, Salinas Valley, Kennedy Space Center, and University of Pavia HSI datasets. To optimize the network for the FPGA, pruning and quantization were employed to reduce the precision from a 32-bit floating-point to an 8-bit integer representation.

Experimental results showed that the CAE achieved an average inference time of 4 ms per 144x144 HSI image on the ZCU104 board, outperforming implementations on a Jetson Xavier NX GPU, with speedups of 4.7x and 2.6x for 16-bit floating-point and 8-bit integer representations, respectively. Furthermore, the FPGA implementation demonstrated superior energy efficiency, consuming 21.52 mJ and outperforming the Jetson Xavier NX GPU by 7.2x and 3.6x.

3.44 An energy-efficient dehazing neural network accelerator based on E^2AOD -Net

Zhang et al. (2024) [185] proposed E^2AOD -Net, a real-time image dehazing NN, and an FPGA-based NN accelerator designed for its implementation. E^2AOD -Net was adapted from AOD-Net [99] and leveraged several optimizations to achieve real-time performance on a PYNQ Z2 board. These optimizations included quantization, pruning, task parallelization, and pipelining. This NN was trained with the RESIDE [100] dataset and evaluated on D-HAZY [6], NH-HAZE [7], SOTS [100], HSTS [100], and FRIDA [161] datasets.

Experimental results showed that, compared to AOD-Net, E^2AOD -Net achieved superior performance metrics, including higher PSNR, SSIM, and MSE. Moreover, regarding implementation efficiency, E^2AOD -Net required 26 ms to infer one image and consumed 2.491 watts. Notably, compared to the Intel Core i9-13900HX CPU, this implementation demonstrated an execution speedup of 72.885 times and a power consumption reduction of 95.5%. Furthermore, compared to the NVIDIA GeForce RTX

4060 GPU, this implementation, although 2.6 times slower, exhibited a substantial power efficiency gain, consuming 98.1% less power.

3.45 Efficient FPGA-accelerated Convolutional Neural Networks for Cloud Detection on CubeSats

Cratere et al. (2024) [31] implemented four CNNs on the Avnet Ultra96-V2 board for cloud detection. These CNNs were implemented with Vitis AI [5] and the Xilinx B1600 DPU IP core [4]. They comprised of Pixel-Net, Patch-Net, Scene-Net, and a U-Net-based network. Data from Sentinel2 Level-2A (L2A) products [41] was used to train and test these networks. To reduce the memory footprint of these CNNs, Vitis AI performed pruning, introducing sparsity in the networks, and quantization, reducing the arithmetic representation to an 8-bit integer. Consequently, the networks' parameters and operations were reduced by up to 98.6% and 90.7%, respectively.

The results showed that the number of false positives was maintained under 1%, and the accuracy loss was only 0.1-0.3% after pruning and 0.1-0.6% after quantization. Moreover, Scene-Net and U-Net demonstrated the lowest inference time for processing a 256x256 image, with execution times of 17.5 ms and 26.7 ms, respectively.

3.46 On-Orbit AI: Cloud Detection Technique for Resource-Limited Nanosatellite

Kim et al. (2024) [84] proposed a three-stage cloud detection methodology. Initially, fully clouded or clear sky images were filtered using an image uniformity check; subsequently, extreme cases were filtered using the TriCloudNet classifier based on the SqueezeNet architecture [69]. Following this, a U-net-based segmentation was executed to classify each pixel as cloud or not cloud. The TriCloudNet and U-net-based networks were accelerated on FPGAs using HLS. This later NN was optimized for nanosatellites by pruning its parameters. Furthermore, these NNs were trained and tested on a combined dataset comprising 98 x 98 RGB images from the SPARCS [79] and Landsat 8 CCA [70] datasets. A Zynq-7000 series SoC was employed to execute these tests, which is identical to the onboard computer in the 6U-class A-HiREV nanosatellite [180].

Results demonstrated that the optimized approach implemented in hardware achieved a speed-up of 6.21 times compared to the software-only implementation, outperforming acceleration using the Nvidia Jetson Nano board. Notably, this work showed that the multi-stage filtering method reduced processing time and power consumption by approximately 48%. Moreover, this system has the capability to reduce the downlink data volume by 40-50%.

3.47 FPGA-Based Low-Bit and Lightweight Fast Light Field Depth Estimation

Li et al. (2025) [102] proposed L^3FNet , a low-bit, lightweight light field depth estimation network suitable for deployment in spacecraft environments. This network was implemented on a ZCU104 board using FINN. Specifically, the authors employed disparity partitioning preprocessing, two-dimensional network architecture optimization, pruning, and quantization to adapt the network for efficient execution. The proposed quantization scheme utilized 8-bit values in the input layer and 4-bit values for the parameters stored in on-chip memory. The network was trained and evaluated using the 4D LF Benchmark [65] dataset.

Experimental results showed that the L^3FNet system achieved an inference time of 0.272 ms per image, which is 1210 times faster than its floating-point counterpart on an Intel i5-9600k CPU, 40 times faster than the NVIDIA 2060 super GPU, and 33 times faster than the NVIDIA RTX 3090 GPU. Furthermore, the developed system exhibited a power consumption of 9.493 watts, which was found to be 6.5 times lower than that of an Intel i5-9600k CPU, 18 times lower than that of an NVIDIA 2060 super GPU, and 35 times lower than that of an NVIDIA RTX 3090 GPU.

4 OBSERVATIONS AND DISCUSSION

After comprehending the unique contributions of each study, attention shifts toward a broader perspective. This approach facilitates the identification of prevailing trends, existing gaps, and potential directions for future research.

4.1 Type of Neural Networks

Figure 6 illustrates the NN types that have been accelerated using FPGAs for on-board space applications. Notably, classification tasks dominate this domain, accounting for 42% of the NN types employed. These

Distribution of NN Types per Paper

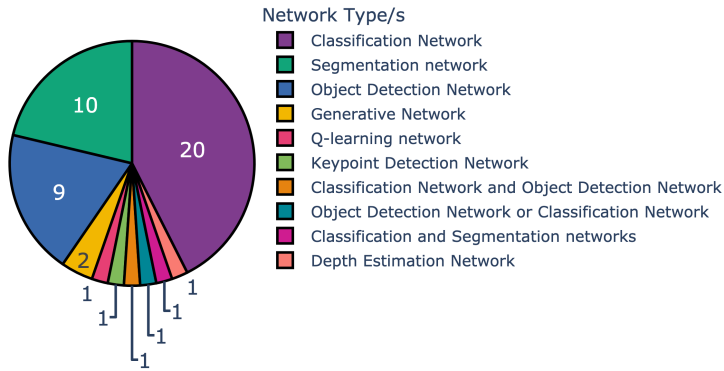


Figure 6. Neural Network types used in the surveyed literature.

tasks are primarily addressed through CNNs, which include both custom architectures and established models such as YOLO, MobileNet, and ResNet. Additionally, segmentation networks represent 21%, while object detection networks account for 19%. Other network types, including Q-learning or generative networks, remain less prevalent. Despite their popularity in language modeling on Earth, transformers have not yet been explored for space applications. The majority of these NN implementations are focused on Earth observation (EO) tasks.

4.2 Training and Learning

The training methodologies for these NNs vary: the majority were trained offline in a supervised manner. Only two papers employed an offline unsupervised approach (sections 3.8 and 3.43), two utilized online supervised training (3.10 and 3.40), and one combined online with unsupervised methods (3.16). The datasets and NNs input primarily consist of remote sensing images from satellite sensors, including RGB, Synthetic Aperture Radar (SAR), and multispectral images. These inputs range from single pixels with 12 spectral bands to full 1024x1024x3 RGB images.

4.3 Size and Parameters

The number of parameters in these NNs varies significantly, ranging from a few hundred to millions, depending on the NN model. This parameter count influences the memory footprint of the NNs, which can be estimated by considering the quantization approach employed. However, this approach may differ between layers within the same NN, complicating the estimation of the memory footprint based solely on parameter count information. Most NNs employ an 8-bit fixed-point arithmetic quantization approach. Nevertheless, two implementations adopted a 1-bit quantization strategy (3.5 and 3.14), and a few others retained 32-bit floating point precision (3.3, 3.6, 3.13, 3.24, 3.27 and 3.32). Although most NNs have a memory footprint under one megabyte or just a few megabytes, the largest reported NN footprint was 49.4 MB (3.35 and 3.38).

Comparing these quantized NNs with their floating-point counterparts, most studies report only a slight degradation in accuracy. Some literature minimizes this degradation by performing Quantization-Aware Training (QAT) or fine-tuning their NN using QAT on a subset of their dataset following Post-Training Quantization (PTQ). Alternatively, some reports employ PTQ exclusively. The literature that does not specify their training approach concerning quantization appears to have predominantly adopted the latter method.

4.4 Implementation Strategies

Most of these NNs were implemented on FPGAs from AMD/Xilinx; only five works used an Altera FPGA (3.11, 3.13, 3.15, 3.28 and 3.35), and two did not disclose their FPGA type. As shown in Figure 7, more implementations leverage HDLs on these FPGAs than other methods. However, the

Distribution of Hardware Description Methods per Paper

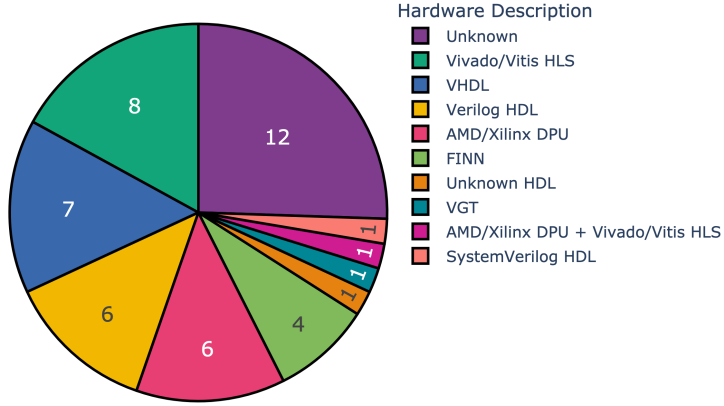


Figure 7. Distribution of hardware description methods used in the surveyed literature.

use of the AMD/Xilinx DPU with Vitis AI for this purpose has increased in recent years, with five out of six such implementations belonging to the last two years. Another important aspect is that from these implementations, 24 accelerators leveraged a time-multiplexed architecture, 18 utilized a dataflow architecture, and five did not describe their logic design. Most of these accelerators operated using a clock signal with either 200 or 100 MHz frequencies, with dataflow accelerators tending to function at lower frequencies than time-multiplexed accelerators. A few accelerators employed two distinct clock signals (3.9, 3.19, 3.20, 3.21, and 3.43), which served as the clock for separate hardware components, such as accelerator interconnects and DSPs.

4.5 Performance and Power-consumption Trends

Inference times for these accelerators ranged from under ten milliseconds to over 100 seconds per image. Due to the lack of batch or pipelined inference implementation in many accelerators, their throughput, expressed as FPS, is the reciprocal of this metric. These metrics are highly influenced by the NN model's operations, parameters, and input size, as illustrated in Figure 8. Conversely, Figure 9 demonstrates that the number of operations per second abstracts from these influences and primarily depends on the accelerator's logic design and FPGA resources utilized. While FPS is critical for mission planning and ensuring optimal performance for specific NN models, the number of operations per second more accurately represents an accelerator's overall performance. This makes it a more suitable measure for comparing accelerators across different applications. Additionally, Figure 9b indicates that dataflow architecture-based accelerators consume fewer BRAMs than those employing time-multiplexed architectures.

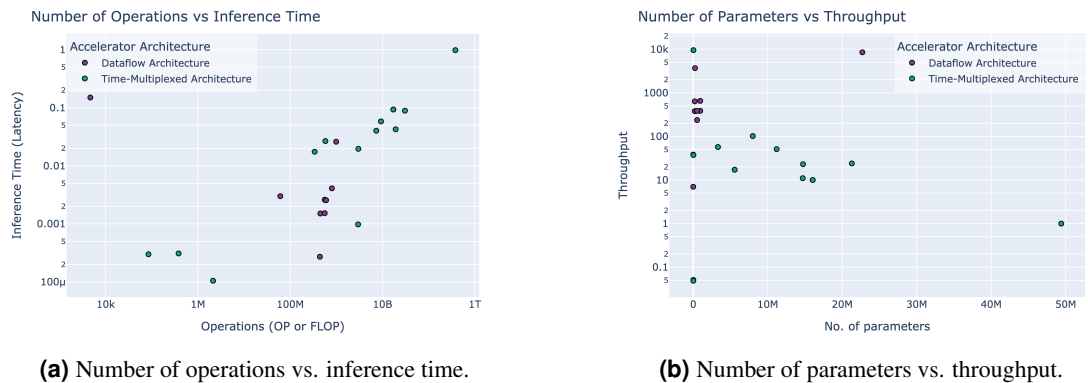


Figure 8. Influence of operations and parameters on inference time and throughput.

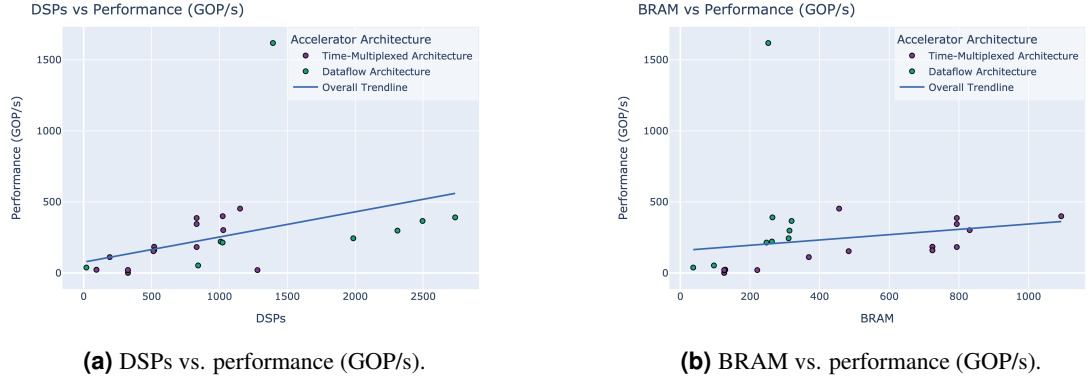


Figure 9. Influence of DSPs and BRAM on performance.

Figure 10 illustrates the general proportionality between operations per second and accelerator power consumption, with some exceptions. This correlation is logical because increased operations per second typically leads to higher resource utilization on an FPGA, resulting in increased power consumption. However, it should be noted that reported power consumptions were often estimated rather than measured, focusing primarily on on-chip or accelerator power. Given its significance for space applications, we advocate reporting measured power consumption. From this metric, we can determine the operations per second per watt, which is particularly valuable for onboard spacecraft implementations as it delineates the relationship between accelerator performance and power efficiency.

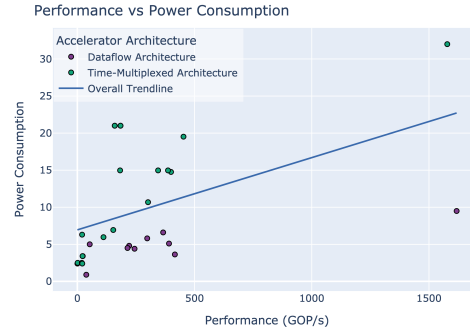


Figure 10. Performance vs. power consumption.

Power consumption is not directly proportional to energy consumption; an accelerator that consumes more power but executes inference faster might consume less energy than one with lower power consumption but longer inference times. While power consumption depends solely on the accelerator architecture, energy consumption also depends on the NN model. Figures 11a and 11b show this dependency and indicate that the number of operations influences energy consumption more than the number of parameters. Consequently, deeper NNs with an increased number of operations necessitate greater energy for inference compared to those with an equivalent parameter count but fewer operations.

Lastly, a few papers in the literature have discussed radiation concerns (3.17, 3.19, 3.22, 3.24, 3.34, 3.38, and 3.39), and even fewer have implemented mechanisms against SEEs (3.9, 3.20, and 3.29). This is a noticeable shortcoming in current implementations. While some missions may not require additional precautions and can neglect these concerns, others might necessitate radiation-tolerant hardware. Implementing this tolerance could influence NN inference time, throughput, and power consumption.

5 FUTURE DIRECTIONS

The literature review reveals a growing interest in deploying NNs on FPGAs for onboard spacecraft applications, yet several areas require further investigation.

Predominantly, the reviewed studies concentrated on classification networks, particularly CNNs. Future research should broaden its scope to encompass diverse NN architectures, including generative

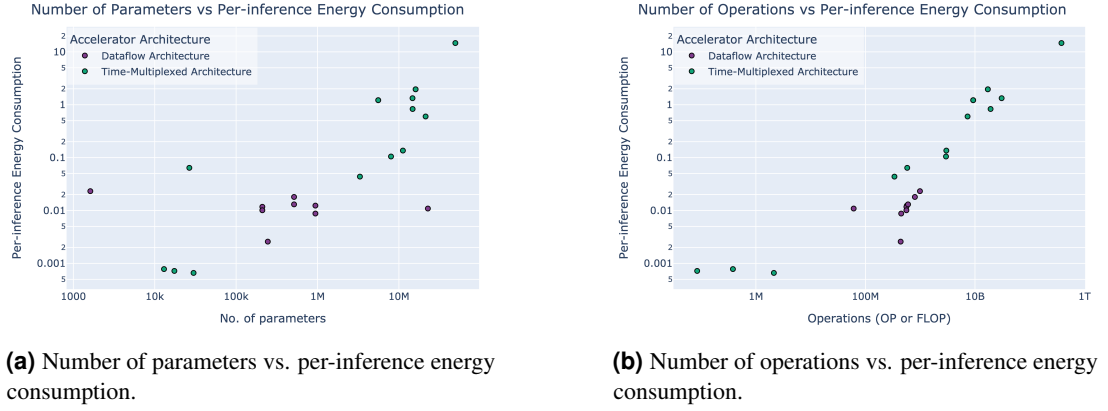


Figure 11. Influence of parameters and operations on per-inference energy consumption.

models and spike-based networks, to address various onboard processing tasks. For instance, generative models could be utilized by partitioning an AutoEncoder into encoder and decoder components: the encoder would operate on the spacecraft, transmitting encoded data to Earth, where the decoder would execute. Additionally, numerous other NN topologies remain unexplored. Notably, none of the reviewed literature supports five-dimensional tensor inputs or 3D convolutions, which are crucial for certain space applications.

Our review reveals that only one study employs online unsupervised learning methods, highlighting a significant gap in this area. Developing NNs capable of online unsupervised learning could enhance adaptability to dynamic environments and reduce reliance on labeled datasets. SNNs can fulfill this role and have demonstrated greater power efficiency than conventional ANNs. However, the literature includes only a few implementations of SNNs, suggesting ample opportunity for further research.

Additionally, the limited attention given to radiation effects in most studies underscores the necessity for research on radiation-tolerant NN accelerators. Future work could address these effects and document the impact of techniques designed to mitigate them.

6 CONCLUSION

This survey presents a comprehensive overview of the current state of FPGA-based NN accelerators for onboard spacecraft applications. It encompasses 47 relevant papers, underscoring the growing interest in this domain and the increasing number of publications in recent years. The analysis reveals that classification networks, particularly CNNs, dominate the literature, focusing predominantly on EO applications. The reviewed studies primarily utilize AMD/Xilinx FPGAs and employ various design methodologies, including time-multiplexed and dataflow architectures.

ACKNOWLEDGMENTS

Open-weights AI models, such as llama3 and phi4, were used locally to revise selected parts of the text within this work to ensure the text is fluid and there are no spelling or grammar errors.

REFERENCES

- [1] ABDERRAHMANE, N., MIRAMOND, B., KERVENNIC, E., AND GIRARD, A. SPLEAT: SPiking Low-power Event-based ArchiTecture for in-orbit processing of satellite imagery. In *2022 International Joint Conference on Neural Networks (IJCNN)* (Padua, Italy, July 2022), IEEE, pp. 1–10.
- [2] ABRAMOVICI, M., EMMERT, J., AND STROUD, C. Roving STARS: An integrated approach to on-line testing, diagnosis, and fault tolerance for FPGAs in adaptive computing systems. In *Proceedings Third NASA/DoD Workshop on Evolvable Hardware. EH-2001* (July 2001), pp. 73–92.
- [3] ABRAMOVICI, M., AND STROUD, C. BIST-based test and diagnosis of FPGA logic blocks. *IEEE Transactions on Very Large Scale Integration (VLSI) Systems* 9, 1 (Feb. 2001), 159–172.

- [4] AMD, X. DPUCZDX8G for Zynq UltraScale+ MPSoCs Product Guide (PG338). https://docs.amd.com/r/en-US/pg338-dpu?tocId=3xsG16y_QFTWvAJKHbisEw, 2025.
- [5] AMD, X. Vitis AI User Guide (UG1414). <https://docs.amd.com/r/en-US/ug1414-vitis-ai>, 2025.
- [6] ANCUTI, C., ANCUTI, C. O., AND DE VLEESCHOUWER, C. D-HAZY: A dataset to evaluate quantitatively dehazing algorithms. In *2016 IEEE International Conference on Image Processing (ICIP)* (Sept. 2016), pp. 2226–2230.
- [7] ANCUTI, C. O., ANCUTI, C., AND TIMOFTE, R. NH-HAZE: An Image Dehazing Benchmark with Non-Homogeneous Hazy and Haze-Free Images. In *2020 IEEE/CVF Conference on Computer Vision and Pattern Recognition Workshops (CVPRW)* (June 2020), pp. 1798–1805.
- [8] ASO, Y., HATTORI, D., YU, Y., JOHNSTON, R. M., IYER, N. A., NGO, T.-T., DIONNE, H., ABBOTT, L.F., AXEL, R., TANIMOTO, H., AND RUBIN, G. M. The neuronal architecture of the mushroom body provides a logic for associative learning. *eLife* 3 (Dec. 2014), e04577.
- [9] BADRINARAYANAN, V., HANDA, A., AND CIPOLLA, R. SegNet: A Deep Convolutional Encoder-Decoder Architecture for Robust Semantic Pixel-Wise Labelling, May 2015.
- [10] BAHL, G., DANIEL, L., MORETTI, M., AND LAFARGE, F. Low-power neural networks for semantic segmentation of satellite images. In *2019 IEEE/CVF INTERNATIONAL CONFERENCE ON COMPUTER VISION WORKSHOPS (ICCVW)* (10662 LOS VAQUEROS CIRCLE, PO BOX 3014, LOS ALAMITOS, CA 90720-1264 USA, 2019), IEEE International Conference on Computer Vision Workshops, IEEE COMPUTER SOC, pp. 2469–2476.
- [11] BARNABY, H. J. Total-Ionizing-Dose Effects in Modern CMOS Technologies. *IEEE Transactions on Nuclear Science* 53, 6 (Dec. 2006), 3103–3121.
- [12] BARTH, J. L. Space and Atmospheric Environments: From Low Earth Orbits to Deep Space. In *Protection of Materials and Structures from Space Environment* (Dordrecht, 2003), J. I. Kleiman and Z. Iskanderova, Eds., Springer Netherlands, pp. 7–29.
- [13] BIAN, L. NWPU VHR-10, July 2023.
- [14] BLOTT, M., PREUSSER, T. B., FRASER, N. J., GAMBARDELLA, G., O'BRIEN, K., UMUROGLU, Y., LEESER, M., AND VISSERS, K. FINN-R: An End-to-End Deep-Learning Framework for Fast Exploration of Quantized Neural Networks. *ACM Transactions on Reconfigurable Technology and Systems* 11, 3 (Dec. 2018), 16:1–16:23.
- [15] BOADA GARDENYES, R. Trends and patterns in ASIC and FPGA use in space missions and impact in technology roadmaps of the European Space Agency.
- [16] BOCHKOVSKIY, A., WANG, C.-Y., AND LIAO, H.-Y. M. YOLOv4: Optimal speed and accuracy of object detection, 2020.
- [17] BURKITT, A. N. A review of the integrate-and-fire neuron model: I. Homogeneous synaptic input. *Biological cybernetics* 95 (2006), 1–19.
- [18] CARMELI, G., AND BEN-MOSHE, B. AI-Based Real-Time Star Tracker. *ELECTRONICS* 12, 9 (May 2023).
- [19] CASTELINO, C., KHANDELWAL, S., SHREEJITH, S., AND BOGARAJU, S. V. An Energy-Efficient Artefact Detection Accelerator on FPGAs for Hyper-Spectral Satellite Imagery, July 2024.
- [20] CHEN, L.-C., PAPANDREOU, G., SCHROFF, F., AND ADAM, H. Rethinking Atrous Convolution for Semantic Image Segmentation, Dec. 2017.
- [21] CHEN, L.-C., ZHU, Y., PAPANDREOU, G., SCHROFF, F., AND ADAM, H. Encoder-Decoder with Atrous Separable Convolution for Semantic Image Segmentation. In *Proceedings of the European Conference on Computer Vision (ECCV)* (2018), pp. 801–818.
- [22] CHEN, X., JI, J., MEI, S., ZHANG, Y., HAN, M., AND DU, Q. FPGA Based Implementation of Convolutional Neural Network for Hyperspectral Classification. In *IGARSS 2018 - 2018 IEEE International Geoscience and Remote Sensing Symposium* (July 2018), pp. 2451–2454.
- [23] CHENG, G., AND HAN, J. A survey on object detection in optical remote sensing images. *ISPRS Journal of Photogrammetry and Remote Sensing* 117 (July 2016), 11–28.
- [24] CHENG, G., HAN, J., AND LU, X. Remote Sensing Image Scene Classification: Benchmark and State of the Art. *Proceedings of the IEEE* 105, 10 (Oct. 2017), 1865–1883.
- [25] CHENG, G., ZHOU, P., AND HAN, J. Learning Rotation-Invariant Convolutional Neural Networks for Object Detection in VHR Optical Remote Sensing Images. *IEEE Transactions on Geoscience and Remote Sensing* 54, 12 (Dec. 2016), 7405–7415.
- [26] CHIEN, S., DOYLE, R., DAVIES, A., JONSSON, A., AND LORENZ, R. The Future of AI in Space.

- IEEE Intelligent Systems* 21, 4 (July 2006), 64–69.
- [27] COCA, M., AND DATCU, M. FPGA Accelerator for Meta-Recognition Anomaly Detection: Case of Burned Area Detection. *IEEE JOURNAL OF SELECTED TOPICS IN APPLIED EARTH OBSERVATIONS AND REMOTE SENSING* 16 (2023), 5247–5259.
 - [28] CONSORTIUM, VIDEO., ET AL. Video imaging demonstrator for earth observation.
 - [29] COSMAS, K., AND KENICHI, A. Utilization of FPGA for Onboard Inference of Landmark Localization in CNN-Based Spacecraft Pose Estimation. *Aerospace* 7, 11 (Nov. 2020), 159.
 - [30] COURBARIAUX, M., HUBARA, I., SOUDRY, D., EL-YANIV, R., AND BENGIO, Y. Binarized Neural Networks: Training Deep Neural Networks with Weights and Activations Constrained to +1 or -1, Mar. 2016.
 - [31] CRATERE, A., FARISSI, M. S., CARBONE, A., ASCIOLLA, M., RIZZI, M., DELL’OLIO, F., NASCETTI, A., AND SPILLER, D. Efficient FPGA-accelerated Convolutional Neural Networks for Cloud Detection on CubeSats.
 - [32] CUI, C., GE, F., LI, Z., YUE, X., ZHOU, F., AND WU, N. Design and Implementation of OpenCL-Based FPGA Accelerator for YOLOv2. In *2021 IEEE 21st International Conference on Communication Technology (ICCT)* (Oct. 2021), pp. 1004–1007.
 - [33] CZAJKOWSKI, T. S., NETO, D., KINSNER, M., AYDONAT, U., WONG, J., DENISENKO, D., YIANNACOURAS, P., FREEMAN, J., SINGH, D. P., AND BROWN, S. D. Opencl for fpgas: Prototyping a compiler. In *Proceedings of the International Conference on Engineering of Reconfigurable Systems and Algorithms (ERSA)* (2012), The Steering Committee of The World Congress in Computer Science, Computer ... , p. 1.
 - [34] DARAM, A. R., KUDITHIPUDI, D., AND YANGUAS-GIL, A. Task-Based Neuromodulation Architecture for Lifelong Learning. In *20th International Symposium on Quality Electronic Design (ISQED)* (Mar. 2019), pp. 191–197.
 - [35] DAVIES, M., SRINIVASA, N., LIN, T.-H., CHINYA, G., CAO, Y., CHODAY, S. H., DIMOU, G., JOSHI, P., IMAM, N., JAIN, S., LIAO, Y., LIN, C.-K., LINES, A., LIU, R., MATHAIKUTTY, D., MCCOY, S., PAUL, A., TSE, J., VENKATARAMANAN, G., WENG, Y.-H., WILD, A., YANG, Y., AND WANG, H. Loihi: A Neuromorphic Manycore Processor with On-Chip Learning. *IEEE Micro* 38, 1 (Jan. 2018), 82–99.
 - [36] DEL ROSSO, M. P., SEBASTIANELLI, A., SPILLER, D., MATHIEU, P. P., AND ULLO, S. L. On-board volcanic eruption detection through cnns and satellite multispectral imagery. *Remote Sensing* 13, 17 (2021), 3479.
 - [37] DRUSCH, M., DEL BELLO, U., CARLIER, S., COLIN, O., FERNANDEZ, V., GASCON, F., HOERSCH, B., ISOLA, C., LABERINTI, P., MARTIMORT, P., MEYGREY, A., SPOTO, F., SY, O., MARCHESE, F., AND BARGELLINI, P. Sentinel-2: ESA’s Optical High-Resolution Mission for GMES Operational Services. *Remote Sensing of Environment* 120 (May 2012), 25–36.
 - [38] DUNG, H. A., CHEN, B., AND CHIN, T.-J. A Spacecraft Dataset for Detection, Segmentation and Parts Recognition. In *Proceedings of the IEEE/CVF Conference on Computer Vision and Pattern Recognition* (2021), pp. 2012–2019.
 - [39] EDMONDS, L., BARNES, C., SCHEICK, L., AERONAUTICS, U. S. N., ADMINISTRATION, S., AND LABORATORY (U.S.), J. P. *An Introduction to Space Radiation Effects on Microelectronics*. JPL Publication. Jet Propulsion Laboratory, National Aeronautics and Space Administration, 2000.
 - [40] EKBLAD, A., MAHENDRAKAR, T., WHITE, R., WILDE, M., SILVER, I., AND WHEELER, B. Resource-constrained FPGA Design for Satellite Component Feature Extraction. In *2023 IEEE AEROSPACE CONFERENCE* (345 E 47TH ST, NEW YORK, NY 10017 USA, 2023), IEEE Aerospace Conference Proceedings, IEEE.
 - [41] ESA, E. S. A. Sentinel 2 Products. <https://sentinwiki.copernicus.eu/web/s2-products>, 2025.
 - [42] EVANS, D., AND MERRI, M. OPS-SAT: A ESA nanosatellite for accelerating innovation in satellite control. In *SpaceOps 2014 Conference* (Pasadena, CA, May 2014), American Institute of Aeronautics and Astronautics.
 - [43] EVANS, D. J. OPS-SAT: Operational Concept for ESA’S First Mission Dedicated to Operational Technology. In *SpaceOps 2016 Conference* (Daejeon, Korea, May 2016), American Institute of Aeronautics and Astronautics.
 - [44] EVERINGHAM, M., VAN GOOL, L., WILLIAMS, C. K. I., WINN, J., AND ZISSERMAN, A. The Pascal Visual Object Classes (VOC) Challenge. *International Journal of Computer Vision* 88, 2

- (June 2010), 303–338.
- [45] FOGA, S., SCARAMUZZA, P. L., GUO, S., ZHU, Z., DILLEY, R. D., BECKMANN, T., SCHMIDT, G. L., DWYER, J. L., JOSEPH HUGHES, M., AND LAUE, B. Cloud detection algorithm comparison and validation for operational Landsat data products. *Remote Sensing of Environment* 194 (June 2017), 379–390.
 - [46] FUKUSHIMA, K. Neocognitron: A self-organizing neural network model for a mechanism of pattern recognition unaffected by shift in position. *Biological Cybernetics* 36, 4 (Apr. 1980), 193–202.
 - [47] GALLEG0, A.-J., PERTUSA, A., AND GIL, P. Automatic ship classification from optical aerial images with convolutional neural networks. *Remote Sensing* 10, 511 (2018).
 - [48] GANKIDI, P. R., AND THANGAVELAUTHAM, J. FPGA Architecture for Deep Learning and its application to Planetary Robotics. In *2017 IEEE AEROSPACE CONFERENCE* (345 E 47TH ST, NEW YORK, NY 10017 USA, 2017), IEEE Aerospace Conference Proceedings, IEEE.
 - [49] GAO, Z., GAO, S., YAO, Y., LIU, Q., ZENG, S., GE, G., WANG, Y., ULLAH, A., AND REVIRIEGO, P. Systematic Reliability Evaluation of FPGA Implemented CNN Accelerators. *IEEE Transactions on Device and Materials Reliability* 23, 1 (Mar. 2023), 116–126.
 - [50] GATTI, A., AND BERTOLINI, A. Sentinel-2 products specification document. *Rapport technique* (2015), 4–7.
 - [51] GE, Z., LIU, S., WANG, F., LI, Z., AND SUN, J. YOLOX: Exceeding YOLO series in 2021. *arXiv preprint arXiv:2107.08430* (2021).
 - [52] GHOLAMI, A., KIM, S., DONG, Z., YAO, Z., MAHONEY, M. W., AND KEUTZER, K. A survey of quantization methods for efficient neural network inference. In *Low-Power Computer Vision*. Chapman and Hall/CRC, 2022, pp. 291–326.
 - [53] GIUFFRIDA, G., DIANA, L., DE GIOIA, F., BENELLI, G., MEONI, G., DONATI, M., AND FANUCCI, L. CloudScout: A Deep Neural Network for On-Board Cloud Detection on Hyperspectral Images. *Remote Sensing* 12, 14 (July 2020), 2205.
 - [54] GUERRISI, G., DEL FRATE, F., AND SCHIAVON, G. Artificial intelligence based on-board image compression for the ϕ -sat-2 mission. *IEEE Journal of Selected Topics in Applied Earth Observations and Remote Sensing* 16 (2023), 8063–8075.
 - [55] GUO, Z. SCIs-Dataset, Mar. 2025.
 - [56] GUO, Z., LIU, K., LIU, W., SUN, X., DING, C., AND LI, S. An Overlay Accelerator of DeepLab CNN for Spacecraft Image Segmentation on FPGA. *REMOTE SENSING* 16, 5 (Mar. 2024).
 - [57] HAMDAN, M. K. VHDL auto-generation tool for optimized hardware acceleration of convolutional neural networks on FPGA (VGT). Master’s thesis, Iowa State University, 2018.
 - [58] HAMILTON, W. L., YING, R., AND LESKOVEC, J. Inductive Representation Learning on Large Graphs. <https://arxiv.org/abs/1706.02216v4>, June 2017.
 - [59] HAMLIN, L., GREEN, R., MOUROULIS, P., EASTWOOD, M., MCCUBBIN, I., WILSON, D., RANDALL, D., DUDIK, M., AND PAINE, C. Imaging spectrometer science measurements for terrestrial ecology: AVIRIS and the Next Generation AVIRIS characteristics and development status. In *NASA Earth Science Technology Conference* (2010), vol. 22.
 - [60] HAMMELL, R. Ships in satellite imagery, 2018.
 - [61] HASHIMOTO, S., SUGIMOTO, Y., HAMAMOTO, K., AND ISHIHAMA, N. Ship Classification from SAR Images Based on Deep Learning. In *INTELLIGENT SYSTEMS AND APPLICATIONS, VOL 1* (GEWERBESTRASSE 11, CHAM, CH-6330, SWITZERLAND, 2018), K. Arai, S. Kapoor, and R. Bhatia, Eds., vol. 868 of *Advances in Intelligent Systems and Computing*, SPRINGER INTERNATIONAL PUBLISHING AG, pp. 18–34.
 - [62] HE, K., ZHANG, X., REN, S., AND SUN, J. Deep residual learning for image recognition, 2015.
 - [63] HEDBERG, S. AI coming of age: NASA uses AI for autonomous space exploration. *IEEE Expert* 12, 3 (May 1997), 13–15.
 - [64] HEINER, J., SELLERS, B., WIRTHLIN, M., AND KALB, J. FPGA partial reconfiguration via configuration scrubbing. In *2009 International Conference on Field Programmable Logic and Applications* (Aug. 2009), pp. 99–104.
 - [65] HONAUER, K., JOHANNSEN, O., KONDERMANN, D., AND GOLDLUECKE, B. A Dataset and Evaluation Methodology for Depth Estimation on 4D Light Fields. In *Computer Vision – ACCV 2016* (Cham, 2017), S.-H. Lai, V. Lepetit, K. Nishino, and Y. Sato, Eds., Springer International Publishing, pp. 19–34.

- [66] HOWARD, A., SANDLER, M., CHU, G., CHEN, L.-C., CHEN, B., TAN, M., WANG, W., ZHU, Y., PANG, R., VASUDEVAN, V., LE, Q. V., AND ADAM, H. Searching for MobileNetV3. In *Proceedings of the IEEE/CVF International Conference on Computer Vision (ICCV)* (Oct. 2019).
- [67] HOWARD, A. G., ZHU, M., CHEN, B., KALENICHENKO, D., WANG, W., WEYAND, T., AND DREETTO, M., AND ADAM, H. MobileNets: Efficient Convolutional Neural Networks for Mobile Vision Applications, Apr. 2017.
- [68] HUANG, L., JIANG, B., LV, S., LIU, Y., AND FU, Y. Deep-Learning-Based Semantic Segmentation of Remote Sensing Images: A Survey. *IEEE Journal of Selected Topics in Applied Earth Observations and Remote Sensing* 17 (2024), 8370–8396.
- [69] IANDOLA, F. N., HAN, S., MOSKEWICZ, M. W., ASHRAF, K., DALLY, W. J., AND KEUTZER, K. SqueezeNet: AlexNet-level accuracy with 50x fewer parameters and 0.5MB model size, 2016.
- [70] IRISH, R. R., BARKER, J. L., GOWARD, S. N., AND ARVIDSON, T. Characterization of the Landsat-7 ETM+ Automated Cloud-Cover Assessment (ACCA) Algorithm. *Photogrammetric Engineering & Remote Sensing* 72, 10 (Oct. 2006), 1179–1188.
- [71] JAIN, A., PITCHIKA, E. D., AND BHARADWAJ, S. An Exploration of FPGA based Multilayer Perceptron using Residue Number System for Space Applications. In *PROCEEDINGS OF 2018 14TH IEEE INTERNATIONAL CONFERENCE ON SIGNAL PROCESSING (ICSP)* (345 E 47TH ST, NEW YORK, NY 10017 USA, 2018), Y. Baozong, R. Qiuqi, Z. Yao, and AN. Gaoyun, Eds., International Conference on Signal Processing, IEEE, pp. 1050–1055.
- [72] JAMES, B. F. *The Natural Space Environment: Effects on Spacecraft*. National Aeronautics and Space Administration, Marshall Space Flight Center, 1994.
- [73] JIAN, T., GONG, Y., ZHAN, Z., SHI, R., SOLTANI, N., WANG, Z., DY, J., CHOWDHURY, K., WANG, Y., AND IOANNIDIS, S. Radio Frequency Fingerprinting on the Edge. *IEEE Transactions on Mobile Computing* 21, 11 (Nov. 2022), 4078–4093.
- [74] JIANG, Q., AND SHA, J. RF Fingerprinting Identification Based on Spiking Neural Network for LEO-MIMO Systems. *IEEE WIRELESS COMMUNICATIONS LETTERS* 12, 2 (Feb. 2023), 287–291.
- [75] JOCHER, G. YOLOv5 by ultralytics, 2020.
- [76] JOHNSON, B. Crowdsourced mapping, 2016.
- [77] JOHNSON, B. A., AND IIZUKA, K. Integrating OpenStreetMap crowdsourced data and Landsat time-series imagery for rapid land use/land cover (LULC) mapping: Case study of the Laguna de Bay area of the Philippines. *Applied Geography* 67 (Feb. 2016), 140–149.
- [78] JONES, H. The Recent Large Reduction in Space Launch Cost.
- [79] KARAKIZI, C., KARANTZALOS, K., VAKALOPOULOU, M., AND ANTONIOU, G. Detailed Land Cover Mapping from Multitemporal Landsat-8 Data of Different Cloud Cover. *Remote Sensing* 10, 8 (Aug. 2018), 1214.
- [80] KERNS, S., SHAFER, B., ROCKETT, L., PRIDMORE, J., BERNDT, D., VAN VONNO, N., AND BARBER, F. The design of radiation-hardened ICs for space: A compendium of approaches. *Proceedings of the IEEE* 76, 11 (Nov. 1988), 1470–1509.
- [81] KESUMA, H., AHMADI-POUR, S., JOSEPH, A., AND WEIS, P. Artificial Intelligence Implementation on Voice Command and Sensor Anomaly Detection for Enhancing Human Habitation in Space Mission. In *2019 9TH INTERNATIONAL CONFERENCE ON RECENT ADVANCES IN SPACE TECHNOLOGIES (RAST)* (345 E 47TH ST, NEW YORK, NY 10017 USA, 2019), IEEE, pp. 579–584.
- [82] KIM, D., JEONG, S., AND KIM, J.-Y. Agamotto: A Performance Optimization Framework for CNN Accelerator With Row Stationary Dataflow. *IEEE Transactions on Circuits and Systems I: Regular Papers* 70, 6 (June 2023), 2487–2496.
- [83] KIM, H., PARK, J., LEE, H., WON, D., AND HAN, M. An FPGA-Accelerated CNN with Parallelized Sum Pooling for Onboard Realtime Routing in Dynamic Low-Orbit Satellite Networks. *Electronics* 13, 12 (Jan. 2024), 2280.
- [84] KIM, J.-H., KIM, Y., CHO, D.-H., AND KIM, S.-M. On-Orbit AI: Cloud Detection Technique for Resource-Limited Nanosatellite. *International Journal of Aeronautical and Space Sciences* (Dec. 2024).
- [85] KISANTAL, M., SHARMA, S., PARK, T. H., IZZO, D., MÄRTENS, M., AND D’AMICO, S. Satellite Pose Estimation Challenge: Dataset, Competition Design and Results. *IEEE Transactions*

- on *Aerospace and Electronic Systems* 56, 5 (Oct. 2020), 4083–4098.
- [86] KOONCE, B. ResNet 50. In *Convolutional Neural Networks with Swift for Tensorflow: Image Recognition and Dataset Categorization*, B. Koonce, Ed. Apress, Berkeley, CA, 2021, pp. 63–72.
 - [87] KOREN, AND SU. Reliability Analysis of N-Modular Redundancy Systems with Intermittent and Permanent Faults. *IEEE Transactions on Computers* C-28, 7 (July 1979), 514–520.
 - [88] KULU, E. Small Launchers - 2023 Industry Survey and Market Analysis. *th International Astronautical Congress* (2023).
 - [89] KUON, I., TESSIER, R., ROSE, J., ET AL. Fpga architecture: Survey and challenges. *Foundations and Trends® in Electronic Design Automation* 2, 2 (2008), 135–253.
 - [90] KYRIAKOS, A., PAPTIOFANOUS, E.-A., BEZAITIS, C., AND REISIS, D. Resources and Power Efficient FPGA Accelerators for Real-Time Image Classification. *JOURNAL OF IMAGING* 8, 4 (Apr. 2022).
 - [91] LECUN, Y., BENGIO, Y., AND HINTON, G. Deep learning. *nature* 521, 7553 (2015), 436–444.
 - [92] LECUN, Y., BENGIO, Y., AND HINTON, G. Deep learning. *Nature* 521, 7553 (May 2015), 436–444.
 - [93] LECUN, Y., BOTTOU, L., BENGIO, Y., AND HAFNER, P. Gradient-based learning applied to document recognition. *Proceedings of the IEEE* 86, 11 (Nov. 1998), 2278–2324.
 - [94] LEMAIRE, E., MORETTI, M., DANIEL, L., MIRAMOND, B., MILLET, P., FERESIN, F., AND BILAVARN, S. An FPGA-based Hybrid Neural Network accelerator for embedded satellite image classification. In *2020 IEEE INTERNATIONAL SYMPOSIUM ON CIRCUITS AND SYSTEMS (ISCAS)* (345 E 47TH ST, NEW YORK, NY 10017 USA, 2020), IEEE International Symposium on Circuits and Systems, IEEE.
 - [95] LENT, R. A Cognitive Network Controller Based on Spiking Neurons. In *2018 IEEE International Conference on Communications (ICC)* (May 2018), pp. 1–6.
 - [96] LENT, R. A Neuromorphic Architecture for Disruption Tolerant Networks. In *2019 IEEE Global Communications Conference (GLOBECOM)* (Dec. 2019), pp. 1–6.
 - [97] LENT, R. Evaluating the Cognitive Network Controller with an SNN on FPGA. In *2020 8TH ANNUAL IEEE INTERNATIONAL CONFERENCE ON WIRELESS FOR SPACE AND EXTREME ENVIRONMENTS (WISEE 2020)* (345 E 47TH ST, NEW YORK, NY 10017 USA, 2020), International Conference on Wireless for Space and Extreme Environments, IEEE, pp. 106–111.
 - [98] LEON, V., LENTARIS, G., SOUDRIS, D., VELLAS, S., AND BERNOU, M. Towards Employing FPGA and ASIP Acceleration to Enable Onboard AI/ML in Space Applications. In *2022 IFIP/IEEE 30th International Conference on Very Large Scale Integration (VLSI-SoC)* (Oct. 2022), pp. 1–4.
 - [99] LI, B., PENG, X., WANG, Z., XU, J., AND FENG, D. AOD-Net: All-in-One Dehazing Network. In *2017 IEEE International Conference on Computer Vision (ICCV)* (Oct. 2017), pp. 4780–4788.
 - [100] LI, B., REN, W., FU, D., TAO, D., FENG, D., ZENG, W., AND WANG, Z. Benchmarking Single-Image Dehazing and Beyond. *IEEE Transactions on Image Processing* 28, 1 (Jan. 2019), 492–505.
 - [101] LI, J., QU, C., AND SHAO, J. Ship detection in SAR images based on an improved faster R-CNN. In *2017 SAR in Big Data Era: Models, Methods and Applications (BIGSAR DATA)* (2017), pp. 1–6.
 - [102] LI, J., ZHANG, C., YANG, W., LI, H., WANG, X., ZHAO, C., DU, S., AND LIU, Y. FPGA-Based Low-Bit and Lightweight Fast Light Field Depth Estimation. *IEEE Transactions on Very Large Scale Integration (VLSI) Systems* (2025), 1–14.
 - [103] LI, K., WAN, G., CHENG, G., MENG, L., AND HAN, J. Object detection in optical remote sensing images: A survey and a new benchmark. *ISPRS Journal of Photogrammetry and Remote Sensing* 159 (Jan. 2020), 296–307.
 - [104] LI, L., ZHANG, S., AND WU, J. Efficient Object Detection Framework and Hardware Architecture for Remote Sensing Images. *REMOTE SENSING* 11, 20 (Oct. 2019).
 - [105] LI, W., AND DU, Q. Collaborative Representation for Hyperspectral Anomaly Detection. *IEEE Transactions on Geoscience and Remote Sensing* 53, 3 (Mar. 2015), 1463–1474.
 - [106] LIN, T.-Y., MAIRE, M., BELONGIE, S., BOURDEV, L., GIRSHICK, R., HAYS, J., PERONA, P., RAMANAN, D., ZITNICK, C. L., AND DOLLÁR, P. Microsoft COCO: Common objects in context. *arXiv e-prints*, arXiv:1405.0312 (May 2014), arXiv:1405.0312.
 - [107] LIU, S., AND LUK, W. Towards an Efficient Accelerator for DNN-Based Remote Sensing Image Segmentation on FPGAs. In *2019 29th International Conference on Field Programmable Logic and*

- Applications (FPL)* (Sept. 2019), pp. 187–193.
- [108] LIU, W., ANGUELOV, D., ERHAN, D., SZEGEDY, C., REED, S., FU, C.-Y., AND BERG, A. C. SSD: Single Shot MultiBox Detector. vol. 9905. 2016, pp. 21–37.
 - [109] LIU, W., MA, L., WANG, J., AND XSCHEN, H. Detection of Multiclass Objects in Optical Remote Sensing Images. *IEEE Geoscience and Remote Sensing Letters* 16, 5 (May 2019), 791–795.
 - [110] LIU, Z., YUAN, L., WENG, L., AND YANG, Y. A high resolution optical satellite image dataset for ship recognition and some new baselines. In *Proceedings of the 6th International Conference on Pattern Recognition Applications and Methods - Volume 1: ICPRAM*, (2017), SciTePress / INSTICC, pp. 324–331.
 - [111] MA, N., YU, X., PENG, Y., AND WANG, S. A Lightweight Hyperspectral Image Anomaly Detector for Real-Time Mission. *Remote Sensing* 11, 13 (Jan. 2019), 1622.
 - [112] MAAS, A. L., HANNUN, A. Y., NG, A. Y., ET AL. Rectifier nonlinearities improve neural network acoustic models. In *Proc. Icml* (2013), vol. 30, Atlanta, GA, p. 3.
 - [113] MAASS, W. Networks of spiking neurons: The third generation of neural network models. *Neural Networks* 10, 9 (Dec. 1997), 1659–1671.
 - [114] MAHENDRAKAR, T., HOLMBERG, S., EKBLAD, A., CONTI, E., WHITE, R. T., WILDE, M., AND SILVER, I. Autonomous Rendezvous with Non-cooperative Target Objects with Swarm Chasers and Observers, Jan. 2023.
 - [115] MAZOUZ, A., AND BRIDGES, C. P. Adaptive Hardware Reconfiguration for Performance Tradeoffs in CNNs. In *2019 NASA/ESA Conference on Adaptive Hardware and Systems (AHS)* (July 2019), pp. 33–40.
 - [116] MAZOUZ, A., AND BRIDGES, C. P. Automated CNN back-propagation pipeline generation for FPGA online training. *Journal of Real-Time Image Processing* 18, 6 (Dec. 2021), 2583–2599.
 - [117] MAZOUZ, A. E., AND NGUYEN, V.-T. Online continual streaming learning for embedded space applications. *JOURNAL OF REAL-TIME IMAGE PROCESSING* 21, 3 (May 2024).
 - [118] MCCULLOCH, W. S., AND PITTS, W. A logical calculus of the ideas immanent in nervous activity. *The bulletin of mathematical biophysics* 5, 4 (Dec. 1943), 115–133.
 - [119] MELLIER, Y., RACCA, G., AND LAUREIJS, R. Unveiling the dark universe with the euclid space mission. In *42nd COSPAR Scientific Assembly* (July 2018), vol. 42, pp. E1.16–2–18.
 - [120] MICHEL, F., TREVISAN, M., GIORDANO, D., AND BONAVENTURE, O. A first look at starlink performance. In *Proceedings of the 22nd ACM Internet Measurement Conference* (2022), pp. 130–136.
 - [121] MISRA, D. Mish: A self regularized non-monotonic activation function, 2020.
 - [122] MITTAL, S. A survey of FPGA-based accelerators for convolutional neural networks. *Neural Computing and Applications* 32, 4 (Feb. 2020), 1109–1139.
 - [123] MOHAJERANI, S., AND SAEEDI, P. Cloud-Net: An End-To-End Cloud Detection Algorithm for Landsat 8 Imagery. In *IGARSS 2019 - 2019 IEEE International Geoscience and Remote Sensing Symposium* (July 2019), pp. 1029–1032.
 - [124] MOHAJERANI, S., AND SAEEDI, P. Cloud-net+: A cloud segmentation CNN for landsat 8 remote sensing imagery optimized with filtered jaccard loss function. vol. 2001.08768 of *arXiv*.
 - [125] MORALES, G., HUAMÁN, S. G., AND TELLES, J. Cloud Detection in High-Resolution Multispectral Satellite Imagery Using Deep Learning. In *Artificial Neural Networks and Machine Learning – ICANN 2018* (Cham, 2018), V. Kůrková, Y. Manolopoulos, B. Hammer, L. Iliadis, and I. Maglogiannis, Eds., Springer International Publishing, pp. 280–288.
 - [126] MOUSOULIOTIS, P., TAMPOURATZIS, N., AND PAPAESTATHIOU, I. SqueezeJet-3: An HLS-based Accelerator for Edge CNN Applications on SoC FPGAs. In *2023 XXIX International Conference on Information, Communication and Automation Technologies (ICAT)* (June 2023), pp. 1–6.
 - [127] MOVIDIUS, I. Intel® Movidius™ Myriad™ 2 Vision Processing Unit 4GB - Product Specifications. <https://www.intel.com/content/www/us/en/products/sku/122461/intel-movidius-myriad-2-vision-processing-unit-4gb/specifications.html>, 2020.
 - [128] NERIS, R., RODRIGUEZ, A., GUERRA, R., LOPEZ, S., AND SARMIENTO, R. FPGA-Based Implementation of a CNN Architecture for the On-Board Processing of Very High-Resolution Remote Sensing Images. *IEEE JOURNAL OF SELECTED TOPICS IN APPLIED EARTH OBSERVATIONS AND REMOTE SENSING* 15 (2022), 3740–3750.
 - [129] NGO, D., AND HARRIS, M. A reliable infrastructure based on COTS technology for affordable

- space application. In *2001 IEEE Aerospace Conference Proceedings (Cat. No.01TH8542)* (Mar. 2001), vol. 5, pp. 2435–2441 vol.5.
- [130] NI, S., WEI, X., ZHANG, N., AND CHEN, H. Algorithm-Hardware Co-Optimization and Deployment Method for Field-Programmable Gate-Array-Based Convolutional Neural Network Remote Sensing Image Processing. *REMOTE SENSING* 15, 24 (Dec. 2023).
 - [131] O'BRIEN, F. *The Apollo guidance computer: Architecture and operation*. Springer, 2010.
 - [132] OUELLETTE, M., VENKATA, M. C., PHILOFSKY, B., MATHARU, H., DADA, F., THIAGARAJAN, A., NI, N., KOEHN, R., AND RIVOALLON, F. System-level benefits of the versal platform. *Xilinx WP539 (v1. 2)* (2022).
 - [133] PACINI, T., RAPUANO, E., DINELLI, G., AND FANUCCI, L. A Multi-Cache System for On-Chip Memory Optimization in FPGA-Based CNN Accelerators. *ELECTRONICS* 10, 20 (Oct. 2021).
 - [134] PAPATHEOFANOUS, E. A., TZIOLOS, PH., KALEKIS, V., AMROU, TZ., KONSTANTOULAKIS, G., VENITOURAKIS, G., AND REISIS, D. SoC FPGA Acceleration for Semantic Segmentation of Clouds in Satellite Images. In *PROCEEDINGS OF THE 2022 IFIP/IEEE 30TH INTERNATIONAL CONFERENCE ON VERY LARGE SCALE INTEGRATION (VLSI-SOC)* (345 E 47TH ST, NEW YORK, NY 10017 USA, 2022), IEEE.
 - [135] PAPPALARDO, A. Xilinx/brevitas. Zenodo, 2023.
 - [136] PERRYMAN, N., WILSON, C., AND GEORGE, A. Evaluation of Xilinx Versal Architecture for Next-Gen Edge Computing in Space. In *2023 IEEE AEROSPACE CONFERENCE* (345 E 47TH ST, NEW YORK, NY 10017 USA, 2023), IEEE Aerospace Conference Proceedings, IEEE.
 - [137] PITONAK, R., MUCHA, J., DOBIS, L., JAVORKA, M., AND MARUSIN, M. CloudSatNet-1: FPGA-Based Hardware-Accelerated Quantized CNN for Satellite On-Board Cloud Coverage Classification. *Remote Sensing* 14, 13 (Jan. 2022), 3180.
 - [138] PITSIS, G., TSAGKATAKIS, G., KOZANITIS, C., KALOMOIRIS, I., IOANNOU, A., DOLLAS, A., KATEVENIS, M. G. H., AND TSAKALIDES, P. Efficient Convolutional Neural Network Weight Compression for Space Data Classification on Multi-fpga Platforms. In *2019 IEEE INTERNATIONAL CONFERENCE ON ACOUSTICS, SPEECH AND SIGNAL PROCESSING (ICASSP)* (345 E 47TH ST, NEW YORK, NY 10017 USA, 2019), International Conference on Acoustics Speech and Signal Processing ICASSP, IEEE, pp. 3917–3921.
 - [139] PODOBAS, A., SANO, K., AND MATSUOKA, S. A survey on coarse-grained reconfigurable architectures from a performance perspective. *IEEE Access* 8 (2020), 146719–146743.
 - [140] POPESCU, M.-C., BALAS, V. E., PERESCU-POPESCU, L., AND MASTORAKIS, N. Multilayer Perceptron and Neural Networks.
 - [141] POTSDAM, ISPRS. 2d semantic labeling dataset. *Accessed: Apr* (2018).
 - [142] PRITT, M., AND CHERN, G. Satellite image classification with deep learning. In *2017 IEEE applied imagery pattern recognition workshop (AIPR)* (2017), IEEE, pp. 1–7.
 - [143] RACCA, G. D., LAUREIJS, R., STAGNARO, L., SALVIGNOL, J. C., ALVAREZ, J. L., CRIADO, G. S., VENANCIO, L. G., SHORT, A., STRADA, P., BOENKE, T., COLOMBO, C., CALVI, A., MAIORANO, E., PIERSANTI, O., PREZELUS, S., ROSATO, P., PINEL, J., ROZEMEIJER, H., LESNA, V., MUSI, P., SIAS, M., ANSELM, A., CAZAUBIEL, V., VAILLON, L., MELLIER, Y., AMIAUX, J., BERTHE, M., SAUVAGE, M., AZZOLLINI, R., CROPPER, M., POTTINGER, S., JAHNKE, K., EALET, A., MACIASZEK, T., PASIAN, F., ZACCHEI, A., SCARAMELLA, R., HOAR, J., KOHLEY, R., VAVREK, R., RUDOLPH, A., AND SCHMIDT, M. The Euclid mission design. p. 990400.
 - [144] RAPUANO, E., MEONI, G., PACINI, T., DINELLI, G., FURANO, G., GIUFFRIDA, G., AND FANUCCI, L. An FPGA-Based Hardware Accelerator for CNNs Inference on Board Satellites: Benchmarking with Myriad 2-Based Solution for the CloudScout Case Study. *Remote Sensing* 13, 8 (Jan. 2021), 1518.
 - [145] REDMON, J., AND FARHADI, A. YOLOv3: An Incremental Improvement, Apr. 2018.
 - [146] REED, I., AND YU, X. Adaptive multiple-band CFAR detection of an optical pattern with unknown spectral distribution. *IEEE Transactions on Acoustics, Speech, and Signal Processing* 38, 10 (Oct. 1990), 1760–1770.
 - [147] REITER, P., KARAGIANNAKIS, P., IRELAND, M., GREENLAND, S., AND CROCKETT, L. FPGA acceleration of a quantized neural network for remote-sensed cloud detection. In *7th International Workshop on On-Board Payload Data Compression* (Virtual, Sept. 2020).

- [148] ROLNICK, D., AHUJA, A., SCHWARZ, J., LILICRAP, T., AND WAYNE, G. Experience replay for continual learning. In *Advances in Neural Information Processing Systems* (2019), H. Wallach, H. Larochelle, A. Beygelzimer, F. dAlché-Buc, E. Fox, and R. Garnett, Eds., vol. 32, Curran Associates, Inc.
- [149] SABOGAL, S., GEORGE, A., AND CRUM, G. ReCoN: A Reconfigurable CNN Acceleration Framework for Hybrid Semantic Segmentation on Hybrid SoCs for Space Applications. In *2019 IEEE SPACE COMPUTING CONFERENCE (SCC)* (10662 LOS VAQUEROS CIRCLE, PO BOX 3014, LOS ALAMITOS, CA 90720-1264 USA, 2019), IEEE COMPUTER SOC, pp. 41–52.
- [150] SABOGAL, S., GEORGE, A., AND CRUM, G. Reconfigurable Framework for Resilient Semantic Segmentation for Space Applications. *ACM TRANSACTIONS ON RECONFIGURABLE TECHNOLOGY AND SYSTEMS* 14, 4 (Dec. 2021).
- [151] SANDLER, M., HOWARD, A., ZHU, M., ZHMOGINOV, A., AND CHEN, L.-C. MobileNetV2: Inverted Residuals and Linear Bottlenecks, Mar. 2019.
- [152] SHAO, Y., SHANG, J., LI, Y., DING, Y., ZHANG, M., REN, K., AND LIU, Y. A Configurable Accelerator for CNN-Based Remote Sensing Object Detection on FPGAs. *IET Computers & Digital Techniques* 2024, 1 (2024), 4415342.
- [153] SHIH, F. Y., AND CHENG, S. Automatic seeded region growing for color image segmentation. *Image and Vision Computing* 23, 10 (Sept. 2005), 877–886.
- [154] SIMONYAN, K., AND ZISSERMAN, A. Very deep convolutional networks for large-scale image recognition, 2015.
- [155] SIROSH, J. Planet-Scale Land Cover Classification with FPGAs. In *KDD'18: PROCEEDINGS OF THE 24TH ACM SIGKDD INTERNATIONAL CONFERENCE ON KNOWLEDGE DISCOVERY & DATA MINING* (1515 BROADWAY, NEW YORK, NY 10036-9998 USA, 2018), ASSOC COMPUTING MACHINERY, p. 2877.
- [156] (SNL), S. N. L. MSTAR Dataset. <https://www.sdms.afrl.af.mil/index.php?collection=mstar>, Sept. 1995.
- [157] STIVAKTAKIS, R., TSAGKATAKIS, G., MORAES, B., ABDALLA, F., STARCK, J.-L., AND TSAKALIDES, P. Convolutional Neural Networks for Spectroscopic Redshift Estimation on Euclid Data. *IEEE Transactions on Big Data* 6, 3 (Sept. 2020), 460–476.
- [158] SUMBUL, G., CHARFUELAN, M., DEMIR, B., AND MARKL, V. Bigearthnet: A Large-Scale Benchmark Archive for Remote Sensing Image Understanding. In *IGARSS 2019 - 2019 IEEE International Geoscience and Remote Sensing Symposium* (July 2019), pp. 5901–5904.
- [159] SUMBUL, G., DE WALL, A., KREUZIGER, T., MARCELINO, F., COSTA, H., BENEVIDES, P., CAETANO, M., DEMIR, B., AND MARKL, V. BigEarthNet-MM: A Large-Scale, Multimodal, Multilabel Benchmark Archive for Remote Sensing Image Classification and Retrieval [Software and Data Sets]. *IEEE Geoscience and Remote Sensing Magazine* 9, 3 (Sept. 2021), 174–180.
- [160] SZEGEDY, C., LIU, W., JIA, Y., SERMANET, P., REED, S., ANGUELOV, D., ERHAN, D., VAN-DOUCHE, V., AND RABINOVICH, A. Going deeper with convolutions. In *2015 IEEE Conference on Computer Vision and Pattern Recognition (CVPR)* (June 2015), pp. 1–9.
- [161] TAREL, J.-P., HAUTIERE, N., CORD, A., GRUYER, D., AND HALMAOUI, H. Improved visibility of road scene images under heterogeneous fog. In *2010 IEEE Intelligent Vehicles Symposium* (June 2010), pp. 478–485.
- [162] UG190, X. Virtex-5 FPGA user guide. *UG190* 5 (2009).
- [163] UMUROGLU, Y., FRASER, N. J., GAMBARDILLA, G., BLOTT, M., LEONG, P., JAHRE, M., AND VISSERS, K. FINN: A Framework for Fast, Scalable Binarized Neural Network Inference. In *Proceedings of the 2017 ACM/SIGDA International Symposium on Field-Programmable Gate Arrays* (New York, NY, USA, Feb. 2017), FPGA '17, Association for Computing Machinery, pp. 65–74.
- [164] UNDERWOOD, C., PELLEGRINO, S., LAPPAS, V. J., BRIDGES, C. P., AND BAKER, J. Using CubeSat/micro-satellite technology to demonstrate the Autonomous Assembly of a Reconfigurable Space Telescope (AAReST). *Acta Astronautica* 114 (Sept. 2015), 112–122.
- [165] VITIS, AI. Vitis AI user guide (UG1414 v2. 0). *AMD Xilinx* (2022).
- [166] WANG, H., LI, D., AND ISSHIKI, T. Reconfigurable CNN Accelerator Embedded in Instruction Extended RISC-V Core. In *2023 6th International Conference on Electronics Technology (ICET)* (May 2023), pp. 945–954.
- [167] WANG, L., ZHOU, H., BIAN, C., JIANG, K., AND CHENG, X. Hardware Acceleration and

- Implementation of YOLOX-s for On-Orbit FPGA. *ELECTRONICS* 11, 21 (Nov. 2022).
- [168] WANG, X., HAN, Y., LEUNG, V. C. M., NIYATO, D., YAN, X., AND CHEN, X. Convergence of Edge Computing and Deep Learning: A Comprehensive Survey. *IEEE Communications Surveys & Tutorials* 22, 2 (2020), 869–904.
 - [169] WIJCKER, J. J. *Mechanical Vibrations in Spacecraft Design*. Springer Science & Business Media, Apr. 2013.
 - [170] WILSON, C., SABOGAL, S., GEORGE, A., AND GORDON-ROSS, A. Hybrid, adaptive, and reconfigurable fault tolerance. In *2017 IEEE Aerospace Conference* (Mar. 2017), pp. 1–11.
 - [171] WU, Y., DENG, L., LI, G., ZHU, J., AND SHI, L. Spatio-temporal backpropagation for training high-performance spiking neural networks. *Frontiers in Neuroscience* 12 (2018).
 - [172] XIA, G.-S., BAI, X., DING, J., ZHU, Z., BELONGIE, S., LUO, J., DATCU, M., PELILLO, M., AND ZHANG, L. DOTA: A Large-scale Dataset for Object Detection in Aerial Images, May 2019.
 - [173] XIA, G.-S., HU, J., HU, F., SHI, B., BAI, X., ZHONG, Y., ZHANG, L., AND LU, X. AID: A benchmark data set for performance evaluation of aerial scene classification. *IEEE Transactions on Geoscience and Remote Sensing* 55, 7 (2017), 3965–3981.
 - [174] YAN, T., ZHANG, N., LI, J., LIU, W., AND CHEN, H. Automatic Deployment of Convolutional Neural Networks on FPGA for Spaceborne Remote Sensing Application. *Remote Sensing* 14, 13 (Jan. 2022), 3130.
 - [175] YANG, G., LEI, J., XIE, W., FANG, Z., LI, Y., WANG, J., AND ZHANG, X. Algorithm/Hardware Codesign for Real-Time On-Satellite CNN-Based Ship Detection in SAR Imagery. *IEEE Transactions on Geoscience and Remote Sensing* 60 (2022), 1–18.
 - [176] YANG, Y., AND NEWSAM, S. Bag-of-visual-words and spatial extensions for land-use classification. In *Proceedings of the 18th SIGSPATIAL International Conference on Advances in Geographic Information Systems* (New York, NY, USA, 2010), Gis '10, Association for Computing Machinery, pp. 270–279.
 - [177] YANGUAS-GIL, A., MANE, A., ELAM, J. W., WANG, F., SEVERA, W., DARAM, A. R., AND KUDITHIPUDI, D. The insect brain as a model system for low power electronics and edge processing applications. In *2019 IEEE SPACE COMPUTING CONFERENCE (SCC)* (10662 LOS VAQUEROS CIRCLE, PO BOX 3014, LOS ALAMITOS, CA 90720-1264 USA, 2019), IEEE COMPUTER SOC, pp. 60–66.
 - [178] YARZADA, R., SINGH, D., AND AL-ASAAD, H. A Brief Survey of Fault Tolerant Techniques for Field Programmable Gate Arrays. In *2022 IEEE 12th Annual Computing and Communication Workshop and Conference (CCWC)* (Jan. 2022), pp. 0823–0828.
 - [179] YU, Y., WU, C., ZHAO, T., WANG, K., AND HE, L. OPU: An FPGA-Based Overlay Processor for Convolutional Neural Networks. *IEEE Transactions on Very Large Scale Integration (VLSI) Systems* 28, 1 (Jan. 2020), 35–47.
 - [180] ZELEKE, D. A., AND KIM, H.-D. A New Strategy of Satellite Autonomy with Machine Learning for Efficient Resource Utilization of a Standard Performance CubeSat. *Aerospace* 10, 1 (Jan. 2023), 78.
 - [181] ZHAI, J., LI, B., LV, S., AND ZHOU, Q. FPGA-Based Vehicle Detection and Tracking Accelerator. *Sensors* 23, 4 (Jan. 2023), 2208.
 - [182] ZHANG, B., KANNAN, R., PRASANNA, V., AND BUSART, C. Accurate, Low-latency, Efficient SAR Automatic Target Recognition on FPGA. In *2022 32ND INTERNATIONAL CONFERENCE ON FIELD-PROGRAMMABLE LOGIC AND APPLICATIONS, FPL* (10662 LOS VAQUEROS CIRCLE, PO BOX 3014, LOS ALAMITOS, CA 90720-1264 USA, 2022), International Conference on Field Programmable Logic and Applications, IEEE COMPUTER SOC, pp. 1–8.
 - [183] ZHANG, N., WEI, X., CHEN, H., AND LIU, W. FPGA Implementation for CNN-Based Optical Remote Sensing Object Detection. *ELECTRONICS* 10, 3 (Feb. 2021).
 - [184] ZHANG, Y., WANG, Z., HUANG, Y., REN, J., YIN, Y., LIU, Y., PEDERSEN, G. F., AND SHEN, M. Deep neural network-based receiver for next-generation leo satellite communications. *IEEE Access* 8 (2020), 222109–222116.
 - [185] ZHANG, Z., DU, G., LI, Z., KANG, Q., ZHAO, W., AND WANG, X. An energy-efficient dehazing neural network accelerator based on E²S²AOD-Net. *Journal of Real-Time Image Processing* 21, 6 (Nov. 2024), 197.
 - [186] ZHAO, Y., LV, Y., AND LI, C. Hardware Acceleration of Satellite Remote Sensing Image Object

- Detection Based on Channel Pruning. *APPLIED SCIENCES-BASEL* 13, 18 (Sept. 2023).
- [187] ZHUANG, H., AND LOW, K. S. Real Time Runway Detection in Satellite Images Using Multi-Channel PCNN. In *PROCEEDINGS OF THE 2014 9TH IEEE CONFERENCE ON INDUSTRIAL ELECTRONICS AND APPLICATIONS (ICIEA)* (345 E 47TH ST, NEW YORK, NY 10017 USA, 2014), IEEE Conference on Industrial Electronics and Applications, IEEE, pp. 253+.